Table 1 Echocardiographic data for sham-operated and operated Lmna$^{+/+}$ and Lmna$^{H222P/H222P}$ mice

	IVSd (mm)	PWd (mm)	LVM (mg)	LVEDD (mm)	LVESD (mm)	LVFS (%)	LVEF (%)	Heart rate (beats/min)
Data for male mice aged 3–4, 6–7, and 9–10 months								
3–4 months of age								
Sham-*Lmna*$^{+/+}$ ($n = 12$)	0.47 ± 0.01	0.52 ± 0.02	38.3 ± 2.40	2.99 ± 0.07	1.74 ± 0.04	41.7 ± 0.70	79.4 ± 0.66	481 ± 18
Cast-*Lmna*$^{+/+}$ ($n = 13$)	0.48 ± 0.01	0.50 ± 0.02	31.4 ± 2.05	2.68 ± 0.09	1.60 ± 0.05	40.4 ± 0.51	78.3 ± 0.60	471 ± 12
Sham-*Lmna*$^{H222P/H222P}$ ($n = 15$)	0.50 ± 0.01	0.49 ± 0.02	44.7 ± 2.08	3.27 ± 0.09*	2.33 ± 0.10***	28.9 ± 1.32***	62.6 ± 1.85***	471 ± 12
Cast-*Lmna*$^{H222P/H222P}$ ($n = 15$)	0.48 ± 0.01	0.47 ± 0.02	39.3 ± 3.22	3.13 ± 0.11††	2.09 ± 0.09†††	33.2 ± 1.35$^{\dagger\dagger\dagger,\#}$	69.4 ± 1.73$^{\dagger\dagger\dagger,\#}$	511 ± 15
6–7 months of age								
Sham-*Lmna*$^{+/+}$ ($n = 12$)	0.48 ± 0.01	0.54 ± 0.03	46.4 ± 2.14	3.27 ± 0.06	1.80 ± 0.06	45.2 ± 1.28	82.1 ± 1.12	488 ± 11
Cast-*Lmna*$^{+/+}$ ($n = 13$)	0.48 ± 0.01	0.51 ± 0.02	39.2 ± 1.84	3.03 ± 0.09	1.76 ± 0.07	42.1 ± 1.04	80.0 ± 1.04	480 ± 11
Sham-*Lmna*$^{H222P/H222P}$ ($n = 15$)	0.48 ± 0.02	0.45 ± 0.02	58.4 ± 3.10	3.98 ± 0.11***	3.28 ± 0.13***	18.0 ± 1.18***	45.0 ± 2.46***	517 ± 17
Cast-*Lmna*$^{H222P/H222P}$ ($n = 14$)	0.47 ± 0.03	0.46 ± 0.02	41.9 ± 2.93$^{\#\#}$	3.30 ± 0.06$^{\dagger,\#\#\#}$	2.34 ± 0.07$^{\dagger\dagger\dagger,\#\#}$	29.2 ± 1.23$^{\dagger\dagger\dagger,\#\#\#}$	63.5 ± 1.71$^{\dagger\dagger\dagger,\#\#\#}$	518 ± 14
9–10 months of age								
Sham-*Lmna*$^{+/+}$ ($n = 12$)	0.54 ± 0.02	0.54 ± 0.03	52.9 ± 3.26	3.38 ± 0.05	1.91 ± 0.03	43.5 ± 0.91	81.0 ± 0.85	494 ± 10
Cast-*Lmna*$^{+/+}$ ($n = 13$)	0.48 ± 0.02	0.53 ± 0.02	41.4 ± 2.04	3.08 ± 0.08	1.78 ± 0.06	43.9 ± 1.05	81.5 ± 1.11	506 ± 12
Sham-*Lmna*$^{H222P/H222P}$ ($n = 5$)	0.39 ± 0.02**	0.33 ± 0.03**	54.1 ± 4.98	4.51 ± 0.22***	3.93 ± 0.23***	12.9 ± 1.79***	33.9 ± 4.41***	484 ± 21
Cast-*Lmna*$^{H222P/H222P}$ ($n = 12$)	0.47 ± 0.01$^{\#\#}$	0.47 ± 0.03$^{\dagger\dagger\dagger,\#\#}$	52.4 ± 1.46†	3.72 ± 0.14$^{\dagger\dagger\dagger,\#\#}$	2.97 ± 0.17$^{\dagger\dagger\dagger,\#\#}$	20.9 ± 1.86$^{\dagger\dagger\dagger,\#}$	50.2 ± 3.59$^{\dagger\dagger\dagger,\#}$	533 ± 14
Data for female mice aged 3–4, 6–7, and 9–10 months								
3–4 months of age								
Sham-*Lmna*$^{+/+}$ ($n = 10$)	0.44 ± 0.01	0.48 ± 0.03	31.7 ± 1.43	2.83 ± 0.08	1.61 ± 0.07	43.3 ± 1.98	80.5 ± 1.72	531 ± 16
OVX-*Lmna*$^{+/+}$ ($n = 11$)	0.48 ± 0.01	0.49 ± 0.03	32.4 ± 2.63	2.75 ± 0.07	1.58 ± 0.05	42.8 ± 1.03	80.6 ± 1.01	514 ± 18
Sham-*Lmna*$^{H222P/H222P}$ ($n = 13$)	0.46 ± 0.02	0.46 ± 0.02	38.6 ± 2.74	3.17 ± 0.12*	2.15 ± 0.12**	32.7 ± 1.51***	68.4 ± 2.12***	508 ± 13
OVX-*Lmna*$^{H222P/H222P}$ ($n = 15$)	0.50 ± 0.02	0.49 ± 0.02	34.5 ± 2.03	2.81 ± 0.08$^{\#}$	1.87 ± 0.07††	32.9 ± 1.53†††	68.9 ± 2.30†††	473 ± 9
6–7 months of age								
Sham-*Lmna*$^{+/+}$ ($n = 9$)	0.44 ± 0.01	0.49 ± 0.04	38.9 ± 1.71	3.16 ± 0.07	1.86 ± 0.04	41.3 ± 0.35	78.8 ± 0.44	483 ± 13
OVX-*Lmna*$^{+/+}$ ($n = 11$)	0.50 ± 0.01	0.51 ± 0.02	43.9 ± 1.98	3.19 ± 0.06	1.83 ± 0.05	42.7 ± 0.84	80.4 ± 0.74	487 ± 18
Sham-*Lmna*$^{H222P/H222P}$ ($n = 13$)	0.45 ± 0.01	0.51 ± 0.02	42.3 ± 1.67	3.24 ± 0.08	2.33 ± 0.10***	28.3 ± 1.70***	61.8 ± 2.45***	515 ± 10
OVX-*Lmna*$^{H222P/H222P}$ ($n = 15$)	0.47 ± 0.01	0.47 ± 0.02	40.7 ± 1.83	3.22 ± 0.05	2.35 ± 0.05†††	27.3 ± 0.84†††	60.5 ± 1.32†††	488 ± 11
9–10 months of age								
Sham-*Lmna*$^{+/+}$ ($n = 9$)	0.52 ± 0.02	0.58 ± 0.04	50.1 ± 2.90	3.23 ± 0.09	1.86 ± 0.06	44.9 ± 1.75	82.2 ± 1.45	486 ± 12
OVX-*Lmna*$^{+/+}$ ($n = 10$)	0.52 ± 0.01	0.55 ± 0.04	48.3 ± 4.66	3.23 ± 0.12	1.84 ± 0.07	43.2 ± 0.97	80.8 ± 1.00	527 ± 11
Sham-*Lmna*$^{H222P/H222P}$ ($n = 9$)	0.46 ± 0.03	0.47 ± 0.03**	56.0 ± 3.10	3.91 ± 0.18**	3.18 ± 0.21***	19.1 ± 2.11***	46.7 ± 3.86***	506 ± 14
OVX-*Lmna*$^{H222P/H222P}$ ($n = 13$)	0.47 ± 0.01	0.45 ± 0.03	46.6 ± 2.06	3.53 ± 0.09	2.76 ± 0.11†††	22.6 ± 1.63†††	52.2 ± 2.85†††	519 ± 13

Cardiac function was evaluated by transthoracic echocardiographic analyses of the left ventricle (LV): the left ventricular mass (LVM) and the percentage of left ventricular ejection fraction (LVEF) and fractional shortening (LVFS) were calculated as follows: [(IVSd+PWd+EDD)3−EDD3] × 1.055 and (LVEDD-LVESD)/LVEDD × 100, respectively.

IVSd, interventricular septal wall thickness in diastole; LVEDD, left ventricular end-diastolic diameter; LVEF, left ventricular ejection fraction; LVESD, left ventricular end-systolic diameter; PWd, posterior wall thickness in diastole.

*$P < 0.05$, **$P < 0.01$, and ***$P < 0.001$, vs. age- and sex-matched Sham-Lmna+/+ mice.

$^{\dagger}P < 0.05$, $^{\dagger\dagger}P < 0.01$, and $^{\dagger\dagger\dagger}P < 0.001$, vs. age- and sex-matched Cast- or OVX-Lmna+/+ mice.

$^{\#}P < 0.05$, $^{\#\#}P < 0.01$, and $^{\#\#\#}P < 0.001$, vs. age- and sex-matched Sham-LmnaH222P/H222P mice.

Table 2 Echocardiographic data from *Lmna*$^{+/+}$ and *Lmna*$^{H222P/H222P}$ mice treated with testosterone or flutamide

	IVSd (mm)	PWd (mm)	LVM (mg)	LVEDD (mm)	LVESD (mm)	LVFS (%)	LVEF (%)	Heart rate (bpm)
Data for mice aged 4 months								
Sham-*Lmna*$^{+/+}$ (male, $n = 5$)	0.55 ± 0.02	0.51 ± 0.02	45.0 ± 3.50	3.12 ± 0.09	1.71 ± 0.09	43.9 ± 0.57	81.4 ± 0.61	511 ± 26
Cast+Testosterone-*Lmna*$^{+/+}$ (male, $n = 5$)	0.53 ± 0.02	0.51 ± 0.02	42.5 ± 2.84	3.06 ± 0.13	1.64 ± 0.05	44.1 ± 0.97	82.2 ± 0.88	496 ± 5
Flutamide-*Lmna*$^{+/+}$ (male, $n = 5$)	0.51 ± 0.03	0.54 ± 0.03	45.7 ± 5.19	3.17 ± 0.09	1.71 ± 0.05	43.0 ± 0.25	80.5 ± 0.18	528 ± 3
Sham-*Lmna*$^{H222P/H222P}$ (male, $n = 19$)	0.52 ± 0.01	0.52 ± 0.02	51.1 ± 2.52	3.41 ± 0.08	2.45 ± 0.07	28.1 ± 0.78	62.2 ± 1.14	492 ± 13
Cast-*Lmna*$^{H222P/H222P}$ (male, $n = 14$)	0.48 ± 0.01	0.56 ± 0.02	48.6 ± 2.55	3.31 ± 0.07	2.27 ± 0.06	32.7 ± 0.76***	69.0 ± 0.92***	523 ± 15
Cast+Testosterone-*Lmna*$^{H222P/H222P}$ (male, $n = 14$)	0.52 ± 0.02	0.55 ± 0.04	50.7 ± 3.76	3.32 ± 0.05	2.21 ± 0.05*	33.4 ± 0.74***	69.0 ± 0.98***	521 ± 13
Flutamide-*Lmna*$^{H222P/H222P}$ (male, $n = 10$)	0.53 ± 0.01	0.55 ± 0.02	55.3 ± 2.79	3.47 ± 0.05	2.47 ± 0.04	28.8 ± 0.39	63.5 ± 0.46	547 ± 11
Sham-*Lmna*$^{+/+}$ (female, $n = 5$)	0.43 ± 0.02	0.54 ± 0.03	37.7 ± 4.08	3.01 ± 0.08	1.67 ± 0.05	43.1 ± 0.63	80.8 ± 0.67	544 ± 8
Testosterone-*Lmna*$^{+/+}$ (female, $n = 5$)	0.46 ± 0.02	0.55 ± 0.02	41.4 ± 2.86	3.08 ± 0.04	1.68 ± 0.02	42.7 ± 0.52	80.9 ± 0.60	564 ± 7
Sham-*Lmna*$^{H222P/H222P}$ (female, $n = 17$)	0.48 ± 0.02	0.56 ± 0.02	45.9 ± 2.11	3.20 ± 0.09	2.22 ± 0.09	32.9 ± 0.74	68.5 ± 1.61	516 ± 11
Testosterone-*Lmna*$^{H222P/H222P}$ (female, $n = 10$)	0.51 ± 0.02	0.56 ± 0.03	47.6 ± 3.43	3.20 ± 0.03	2.24 ± 0.02	32.0 ± 0.66	67.7 ± 0.75	537 ± 12
Data for mice aged 6 months								
Sham-*Lmna*$^{+/+}$ (male, $n = 5$)	0.52 ± 0.04	0.57 ± 0.06	49.5 ± 7.45	3.23 ± 0.06	1.82 ± 0.04	43.7 ± 0.44	81.4 ± 0.41	551 ± 16
Cast+Testosterone-*Lmna*$^{+/+}$ (male, $n = 5$)	0.52 ± 0.02	0.59 ± 0.05	48.3 ± 3.95	3.14 ± 0.06	1.76 ± 0.05	42.2 ± 0.45	80.2 ± 0.48	511 ± 3
Flutamide-*Lmna*$^{+/+}$ (male, $n = 5$)	0.51 ± 0.02	0.60 ± 0.03	50.2 ± 5.28	3.21 ± 0.09	1.82 ± 0.05	43.5 ± 0.32	81.4 ± 0.28	526 ± 8
Sham-*Lmna*$^{H222P/H222P}$ (male, $n = 15$)	0.44 ± 0.02	0.45 ± 0.02	53.4 ± 2.77	3.90 ± 0.11	3.19 ± 0.14	18.7 ± 1.40	46.3 ± 2.63	540 ± 15
Cast-*Lmna*$^{H222P/H222P}$ (male, $n = 13$)	0.44 ± 0.01	0.50 ± 0.02	48.1 ± 2.72	3.54 ± 0.08*	2.53 ± 0.08***	28.5 ± 0.91***	62.7 ± 1.21***	505 ± 14
Cast+Testosterone-*Lmna*$^{H222P/H222P}$ (male, $n = 10$)	0.42 ± 0.03	0.42 ± 0.03	56.7 ± 2.80	4.19 ± 0.12	3.46 ± 0.13	17.5 ± 1.36	44.0 ± 2.89	504 ± 9
Flutamide-*Lmna*$^{H222P/H222P}$ (male, $n = 8$)	0.47 ± 0.02	0.48 ± 0.03	49.9 ± 2.98	3.59 ± 0.05	2.62 ± 0.05**	26.9 ± 0.57***	61.6 ± 0.93***	553 ± 14
Sham-*Lmna*$^{+/+}$ (female, $n = 5$)	0.48 ± 0.01	0.57 ± 0.02	45.9 ± 2.63	3.18 ± 0.06	1.85 ± 0.03	42.0 ± 0.20	80.1 ± 0.18	547 ± 7
Testosterone-*Lmna*$^{+/+}$ (female, $n = 5$)	0.47 ± 0.01	0.61 ± 0.04	46.9 ± 3.55	3.15 ± 0.05	1.79 ± 0.02	43.1 ± 0.36	80.8 ± 0.37	576 ± 17
Sham-*Lmna*$^{H222P/H222P}$ (female, $n = 17$)	0.48 ± 0.01	0.50 ± 0.02	44.6 ± 1.67	3.29 ± 0.06	2.37 ± 0.07	28.3 ± 1.28	62.0 ± 1.86	529 ± 11
Testosterone-*Lmna*$^{H222P/H222P}$ (female, $n = 9$)	0.39 ± 0.03	0.39 ± 0.03	47.3 ± 4.87	3.98 ± 0.13***	3.21 ± 0.14***	19.5 ± 1.23***	48.4 ± 2.33***	528 ± 18

Cardiac function was evaluated by transthoracic echocardiographic analyses of the left ventricle (LV): the left ventricular mass (LVM) and the percentage of left ventricular ejection fraction (LVEF) and fractional shortening (LVFS) were calculated as follows: [(IVSd+PWd+EDD)3−EDD3] × 1.055 and (LVEDD-LVESD)/LVEDD × 100, respectively.

IVSd, interventricular septal wall thickness in diastole; LVEDD, left ventricular end-diastolic diameter; LVEF, left ventricular ejection fraction; LVESD, left ventricular end-systolic diameter; PWd, posterior wall thickness in diastole.

*$P < 0.05$, **$P < 0.01$, and ***$P < 0.001$, vs. age-, sex-, and genotype-matched Sham-operated mice.

3.8 Altered expression of genes and proteins related with cardiac remodelling in hearts from Lmna$^{H222P/H222P}$ mice

Abnormal regulation of gene or protein expression involved in the sarcomere organization, cardiac hormones, proto-oncogene, and extracellular matrix remodelling is associated with DCM and CHF,[22] and SRF is required for the induction of cardiac remodelling-associated genes including *Nppa*, *Nppb*, *Myh7*, and *Fos*.[20] We investigated the gene expression profiles in the hearts from *Lmna*$^{H222P/H222P}$ mice. It was observed that the expression of *Nppa*, *Nppb*, and *Myh7* at the mRNA level was increased in the hearts from sham-operated male *Lmna*$^{H222P/H222P}$ mice, and that the up-regulation was suppressed in the hearts from castrated or flutamide-treated male *Lmna*$^{H222P/H222P}$ mice (*Figure 5*). In addition, significant increase in expression of proto-oncogene *Fos* and extracellular matrix remodelling-related genes, such as *Tgfb1*, *Tgfb2*, and *Col1a2*, was found in the hearts from the sham-operated male *Lmna*$^{H222P/H222P}$ mice, which were suppressed by the castration or flutamide treatment (*Figure 5*). Expression of *Nppa*, *Nppb*, *Myh7*, and *Col1a2* was significantly increased in the hearts from testosterone-treated female *Lmna*$^{H222P/H222P}$ mice (*Figure 5*). Moreover, altered expression of atrial natriuretic peptide and β-myosin heavy chain encoded by *Nppa* and *Myh7*, respectively, was confirmed at the protein levels (see Supplementary material online, *Figure S9*).

3.9 Accumulation of androgen-related proteins in nuclei of cardiomyocytes from Lmna$^{H222P/H222P}$ mice

Next, we investigated the expression of AR in the hearts from *Lmna*$^{+/+}$ and *Lmna*$^{H222P/H222P}$ mice (*Table 2*). Western blot analyses showed an increased expression of AR in both total protein and nuclear extracts from the *Lmna*$^{H222P/H222P}$ hearts, irrespective of gender (*Figure 6A* and *B*). The nuclear accumulation of AR was accompanied by the AR co-factors, SRF and FHL2, in the male *Lmna*$^{H222P/H222P}$ hearts, but not in the female *Lmna*$^{H222P/H222P}$ hearts (*Figure 6C* and *D*). The increased nuclear accumulation of SRF and FHL2 was suppressed in the castrated male *Lmna*$^{H222P/H222P}$ mice, whereas no difference was observed in the expression of AR between sham-operated and castrated male *Lmna*$^{H222P/H222P}$ mice (*Figure 6C*). On the other hand, no nuclear accumulation of AR, SRF, or FHL2 was observed in the soleus muscle from the *Lmna*$^{H222P/H222P}$ mice (see Supplementary material online, *Figure S10*). These observations suggested that the nuclear accumulation of androgen-related proteins was specific to the heart muscle, not the skeletal muscles, in *Lmna*$^{H222P/H222P}$ mice, which was consistent with the findings that the gender difference was observed only for cardiac function and not for skeletal muscle symptoms in the *Lmna*$^{H222P/H222P}$ mice.[10]

4. Discussion

Sex hormones mediate their function by activation of specific receptors. Upon activation, sex hormone receptors translocate into nuclei, where they bind hormone response elements in the regulatory region of target genes, and, together with co-activators and other transcription factors, initiate transcription. In this context, androgens including testosterone mediate their action via AR, and androgen-activated AR exerts its biological effect via complex formation with co-regulators.[23] In this study, we demonstrated the increased expression and nuclear accumulation of AR in the hearts from the DCM patients carrying the p.R225X mutation and the *Lmna*$^{H222P/H222P}$ mice. Quite interestingly, we found concomitantly nuclear accumulation of SRF and FHL2 in cardiomyocytes from the human DCM patients and mice. It was reported that SRF and FHL2 formed a complex with AR to act as co-activators of AR-dependent transcription.[24,25] SRF is required for the induction of cardiac remodelling-related genes including *Nppa*, *Nppb*, *Myh7*, and *Fos*,[20] of which expression was increased in the *Lmna*$^{H222P/H222P}$ hearts. In addition, FHL2 is preferentially expressed in the cardiac muscle and only a little in the skeletal muscles.[26] These observations suggested that the cardiomyocyte-specific nuclear accumulation of AR-FHL2-SRF complex induced by testosterone was involved in the disease progression of DCM caused by specific *LMNA* mutations. It is noteworthy that overexpression of AR accelerated nuclear accumulation of FHL2 and SRF in NRCs in the presence of testosterone, and silencing of FHL2 suppressed the translocation of SRF into the nuclei. It is therefore implied that a blockade of SRF–AR–FHL2 complex formation might be a therapeutic strategy for adverse effect of testosterone in DCM caused by *LMNA* mutation. It may be advocating that a high dose testosterone treatment might not be beneficial for CHF, especially for individuals whose AR expression would be increased in the heart, because nuclear accumulation of AR in the cardiac muscles is associated with higher mortality and severity of cardiac dysfunction.

Significant gender differences in morbidity and mortality of human CHF including DCM has been recognized.[6,27,28] Hormone-replacement therapy appeared to improve survival in post-menopausal women with systolic dysfunction.[29] In addition, it has been demonstrated that males displayed more prominent abnormalities in cardiac function than females, and female-related phenotypes could be mimicked by administration of estradiol in males and ovariectomized females in mice.[8] These observations suggested the role of oestrogen as a cardiac protector. On the other hand, potential influence of androgens on the cardiac hypertrophy and fibrosis in mice was described in some reports,[12,30] and a low dose testosterone supplementation improves cardiac functional capacity in CHF patients.[31] However, the adverse or beneficial role of androgens in cardiovascular risk is not fully understood. In this study, we revealed a deleterious role of testosterone in the progression of DCM in a mouse model caused by the *LMNA* mutations.

Castration significantly improved cardiac function and survival prognosis of the male *Lmna*$^{H222P/H222P}$ mice. Interestingly, ovariectomy also improved survival prognosis, albeit to less extent, of the female *Lmna*$^{H222P/H222P}$ mice. Because a small amount of testosterone is produced in the ovary, it was speculated that a slight improvement of survival prognosis in the ovariectomized female *Lmna*$^{H222P/H222P}$ mice was due to the elimination of ovarian testosterone. We also demonstrated that the testosterone significantly worsened the cardiac function in the castrated male *Lmna*$^{H222P/H222P}$ mice and female *Lmna*$^{H222P/H222P}$ mice, indicating the impact of testosterone on disease progression. Because the increased expression of AR was observed in the hearts from both male and female *Lmna*$^{H222P/H222P}$ mice, it was suggested that the presence of both testosterone and AR played pivotal roles in the cardiac phenotype of *Lmna*$^{H222P/H222P}$ mice.

The up-regulation of extracellular matrix remodelling-related genes in the male *Lmna*$^{H222P/H222P}$ mice was significantly suppressed by the castration or treatment with the AR antagonist. This finding was consistent with the significant inhibition of interstitial fibrosis in the hearts from castrated or flutamide-treated male *Lmna*$^{H222P/H222P}$ mice. On the other hand, a long-term treatment with testosterone increased the cardiac

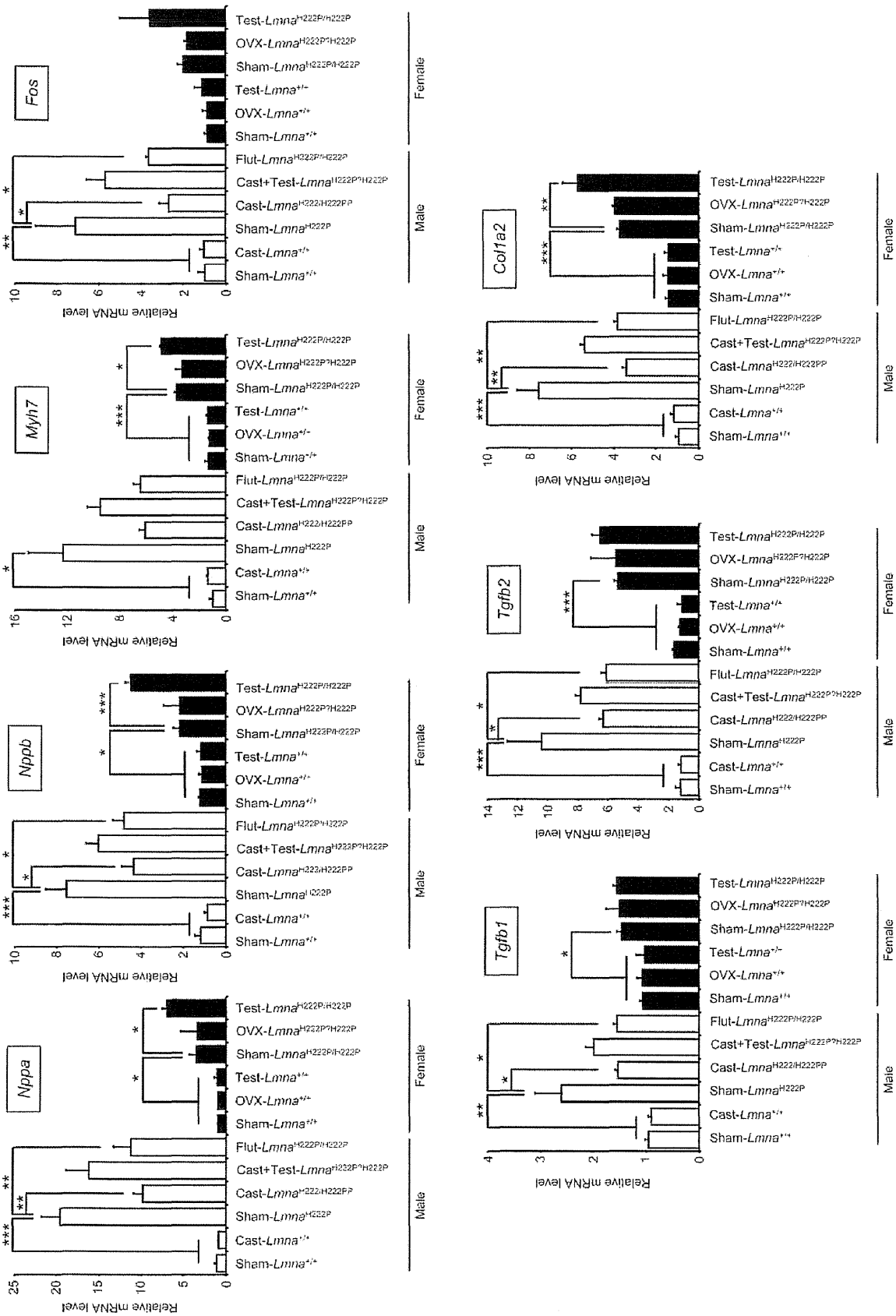

Figure 5 Expression of cardiac remodelling-related genes in LVs from *Lmna*$^{+/+}$ and *Lmna*$^{H222P/H222P}$ mice. Quantitative real-time RT–PCR data showing the steady-state mRNA levels of *Nppa*, *Nppb*, *Myh7*, *Fos*, *Tgfb1*, *Tgfb2*, and *Col1a2*, which encode for atrial natriuretic peptide precursor, brain natriuretic peptide precursor, β-myosin heavy chain, c-fos, TGF-β_1, TGF-β_2, and type I collagen α2 chain, respectively. Bars indicate the mRNA level in LVs normalized to *Gapdh* as calculated by the ΔδCT method. Data are arbitrarily shown as fold-induction and the expression of each gene in LV from a sham-operated *Lmna*$^{+/+}$ mouse was defined as 1.00 AU. Data are expressed as means ± SEM for $n = 6$ per group. Other marks and abbreviations are the same as in the legends to *Figure 4*.

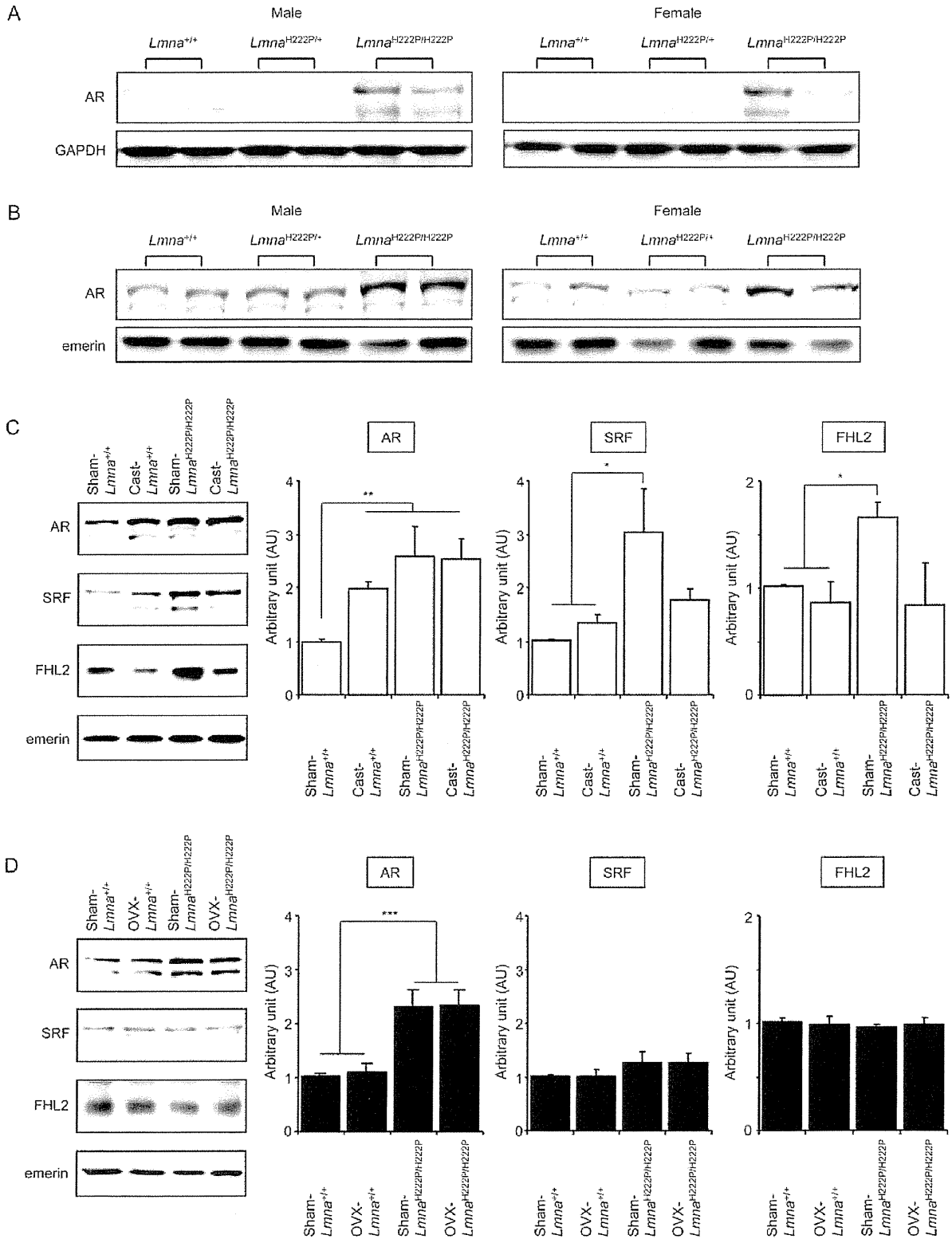

Figure 6 Expression of androgen-related proteins in LVs from mice at 6 months of age. (*A*) Representative immunoblots for AR in total protein extracts from LVs of male and female mice are shown. Labelling with antibody against GAPDH is shown as the loading control. (*B*) Representative immunoblots for AR in nuclear fraction from LV of male and female mice are shown. Labelling with antibody against a nuclear protein, emerin, is shown as the loading control. (*C* and *D*) Expression of AR, SRF, and FHL2 in the nuclear extracts from LVs of sham-operated and operated male (*C*) and female (*D*) mice. Labelling with antibody against emerin is shown as the loading control. Data are arbitrarily shown as fold-inductions and the expression of each protein in LV from a sham-operated $Lmna^{+/+}$ mouse was defined as 1.00 AU. Data are expressed as means ± SEM for $n = 4$ to 8 per group. Other marks and abbreviations are the same as in the legends to *Figure 4*.

fibrosis in the female *Lmna*$^{H222P/H222P}$ mice. It was previously reported that either castration or treatment with flutamide attenuated the cardiac fibrosis in GC-A KO mice.[12] However, nuclear accumulation of AR was not observed in the hearts from the GC-A KO mice in this study. These observations suggested that testosterone played a role in the cardiac remodelling including interstitial fibrosis, but molecular mechanisms underlying the gender difference in the cardiac dysfunction due to the *LMNA* mutations would be different from that caused by the knock-out of the GC-A gene.

There are some limitations in this study. First, it is not resolved how the specific *LMNA* mutations lead to the cardiomyocyte-specific nuclear accumulation of AR. Second, we have not evaluated the angiogenesis in the hearts, which is a hallmark of cardiac remodelling. These issues should be further investigated to elucidate the molecular mechanisms for the gender difference.

In conclusion, we revealed that the nuclear accumulation of AR–FHL2–SRF complex was associated with specific *LMNA* mutations showing the gender difference in disease progression of DCM. We also demonstrated a deleterious effect of testosterone on the DCM phenotypes and survival prognosis in the *Lmna*$^{H222P/H222P}$ mice. Our findings implicated that a blockade of AR signalling might be beneficial for preserving cardiac function in the DCM patients, when nuclear accumulation of AR could be found in their hearts. Nuclear AR accumulation could be a biomarker for prediction of harmful side effects in testosterone supplement therapy for CHF.[31]

Supplementary material

Supplementary material is available at *Cardiovascular Research* online.

Acknowledgements

We are grateful to Prof. K. Taya for helpful discussion about the use of silascon tubes in infusion of testosterone and flutamide. We also thank SRL, Inc. for measuring serum testosterone levels in mice.

Conflict of interest: none declared.

Funding

This work was supported in part by Grant-in-Aids from the Ministry of Education, Culture, Sports, Science and Technology, Japan (grant numbers 22390157, 23132507); grants for Japan–France collaboration research from the Japan Society for the Promotion of Science (JSPS) and the '*Institut National de la Santé et de la Recherche Médicale*' (Inserm); a research grant for Intractable Disease from the Ministry of Health, Labour and Welfare, Japan (grant number 2010-119); a research grant from the 'Association Française contre les Myopathies' (AFM) (grant number 15261); a Grant-in-Aid for SENTAN from the Japan Science and Technology Agency; and the Follow-up grants from the Tokyo Medical and Dental University. This work was also supported by Joint Usage/Research Program of Medical Research Institute, Tokyo Medical and Dental University.

References

1. Richardson P, McKenna W, Bristow M, Maisch B, Mautner B, O'Connell J *et al.* Report of the 1995 World Health Organization/International Society and Federation of Cardiology Task Force on the Definition and Classification of cardiomyopathies. *Circulation* 1996;**93**:841–842.
2. Maron BJ, Towbin JA, Thiene G, Antzelevitch C, Corrado D, Arnett D *et al.* Contemporary definitions and classification of the cardiomyopathies: an American Heart Association Scientific Statement from the Council on Clinical Cardiology, Heart Failure and Transplantation Committee; Quality of Care and Outcomes Research and Functional Genomics and Translational Biology Interdisciplinary Working Groups; and Council on Epidemiology and Prevention. *Circulation* 2006;**113**:1807–1816.
3. Towbin JA, Lowe AM, Colan SD, Sleeper LA, Orav EJ, Clunie S *et al.* Incidence, causes, and outcomes of dilated cardiomyopathy in children. *JAMA* 2006;**296**:1867–1876.
4. Kimura A. Contribution of genetic factors to the pathogenesis of dilated cardiomyopathy: the cause of dilated cardiomyopathy: genetic or acquired? (genetic-side). *Circ J* 2011;**75**:1756–1765.
5. Taylor MR, Fain PR, Sinagra G, Robinson ML, Robertson AD, Carniel E *et al.* Natural history of dilated cardiomyopathy due to lamin A/C gene mutations. *J Am Coll Cardiol* 2003;**41**:771–780.
6. Towbin JA, Bowles NE. The failing heart. *Nature* 2002;**415**:227–233.
7. van Rijsingen IA, Nannenberg EA, Arbustini E, Elliott PM, Mogensen J, Ast JF *et al.* Gender-specific differences in major cardiac events and mortality in lamin A/C mutation carriers. *Eur J Heart Fail* 2013;**15**:376–384.
8. Du XJ. Gender modulates cardiac phenotype development in genetically modified mice. *Cardiovasc Res* 2004;**63**:510–519.
9. Babiker FA, De Windt LJ, van Eickels M, Grohe C, Meyer R, Doevendans PA. Estrogenic hormone action in the heart: regulatory network and function. *Cardiovasc Res* 2002;**53**:709–719.
10. Arimura T, Helbling-Leclerc A, Massart C, Varnous S, Niel F, Lacene E *et al.* Mouse model carrying H222P-Lmna mutation develops muscular dystrophy and dilated cardiomyopathy similar to human striated muscle laminopathies. *Hum Mol Genet* 2005;**14**:155–169.
11. Bertrand AT, Renou L, Papadopoulos A, Beuvin M, Lacene E, Massart C *et al.* DelK32-lamin A/C has abnormal location and induces incomplete tissue maturation and severe metabolic defects leading to premature death. *Hum Mol Genet* 2012;**21**:1037–1048.
12. Li Y, Kishimoto I, Saito Y, Harada M, Kuwahara K, Izumi T *et al.* Androgen contributes to gender-related cardiac hypertrophy and fibrosis in mice lacking the gene encoding guanylyl cyclase-A. *Endocrinology* 2004;**145**:951–958.
13. Montalvo C, Villar AV, Merino D, Garcia R, Ares M, Llano M *et al.* Androgens contribute to sex differences in myocardial remodeling under pressure overload by a mechanism involving TGF-beta. *PLoS ONE* **7**:e35635.
14. Arimura T, Bos JM, Sato A, Kubo T, Okamoto H, Nishi H *et al.* Cardiac ankyrin repeat protein gene (ANKRD1) mutations in hypertrophic cardiomyopathy. *J Am Coll Cardiol* 2009;**54**:334–342.
15. Purevjav E, Arimura T, Augustin S, Huby AC, Takagi K, Nunoda S *et al.* Molecular basis for clinical heterogeneity in inherited cardiomyopathies due to myopalladin mutations. *Hum Mol Genet* 2012;**21**:2039–2053.
16. Li C, Taneda S, Suzuki AK, Furuta C, Watanabe G, Taya K. Anti-androgenic activity of 3-methyl-4-nitrophenol in diesel exhaust particles. *Eur J Pharmacol* 2006;**543**:194–199.
17. Kuwahara M, Chiku K, Shiono T, Tsubone H, Sugano S. ECG changes under hyperkalemia with nephrectomy in the rat. *J Electrocardiol* 1992;**25**:215–219.
18. Arimura T, Sato R, Machida N, Bando H, Zhan DY, Morimoto S *et al.* Improvement of left ventricular dysfunction and of survival prognosis of dilated cardiomyopathy by administration of calcium sensitizer SCH00013 in a mouse model. *J Am Coll Cardiol* 2010;**55**:1503–1505.
19. Muchir A, Pavlidis P, Decostre V, Herron AJ, Arimura T, Bonne G *et al.* Activation of MAPK pathways links LMNA mutations to cardiomyopathy in Emery-Dreifuss muscular dystrophy. *J Clin Invest* 2007;**117**:1282–1293.
20. Nelson TJ, Balza R Jr, Xiao Q, Misra RP. SRF-dependent gene expression in isolated cardiomyocytes: regulation of genes involved in cardiac hypertrophy. *J Mol Cell Cardiol* 2005;**39**:479–489.
21. Niu Z, Li A, Zhang SX, Schwartz RJ. Serum response factor micromanaging cardiogenesis. *Curr Opin Cell Biol* 2007;**19**:618–627.
22. Margulies KB, Bednarik DP, Dries DL. Genomics, transcriptional profiling, and heart failure. *J Am Coll Cardiol* 2009;**53**:1752–1759.
23. Walters KA, Allan CM, Handelsman DJ. Androgen actions and the ovary. *Biol Reprod* 2008;**78**:380–389.
24. Muller JM, Isele U, Metzger E, Rempel A, Moser M, Pscherer A *et al.* FHL2, a novel tissue-specific coactivator of the androgen receptor. *EMBO J* 2000;**19**:359–369.
25. Vlahopoulos S, Zimmer WE, Jenster G, Belaguli NS, Balk SP, Brinkmann AO *et al.* Recruitment of the androgen receptor via serum response factor facilitates expression of a myogenic gene. *J Biol Chem* 2005;**280**:7786–7792.
26. Chan KK, Tsui SK, Lee SM, Luk SC, Liew CC, Fung KP *et al.* Molecular cloning and characterization of FHL2, a novel LIM domain protein preferentially expressed in human heart. *Gene* 1998;**210**:345–350.
27. Adams KF Jr, Dunlap SH, Sueta CA, Clarke SW, Patterson JH, Blauwet MB *et al.* Relation between gender, etiology and survival in patients with symptomatic heart failure. *J Am Coll Cardiol* 1996;**28**:1781–1788.
28. O'Meara E, Clayton T, McEntegart MB, McMurray JJ, Pina IL, Granger CB *et al.* Sex differences in clinical characteristics and prognosis in a broad spectrum of patients with heart failure: results of the Candesartan in Heart failure: Assessment of Reduction in Mortality and morbidity (CHARM) program. *Circulation* 2007;**115**:3111–3120.
29. Lindenfeld J, Ghali JK, Krause-Steinrauf HJ, Khan S, Adams K, Goldman S *et al.* Hormone replacement therapy is associated with improved survival in women with advanced heart failure. *J Am Coll Cardiol* 2003;**42**:1238–1245.
30. Gao XM, Agrotis A, Autelitano DJ, Percy E, Woodcock EA, Jennings GL *et al.* Sex hormones and cardiomyopathic phenotype induced by cardiac beta 2-adrenergic receptor overexpression. *Endocrinology* 2003;**144**:4097–4105.
31. Toma M, McAlister FA, Coglianese EE, Vidi V, Vasaiwala S, Bakal JA *et al.* Testosterone supplementation in heart failure: a meta-analysis. *Circ Heart Fail* 2012;**5**:315–321.

PLOS ONE

An Immunohistochemical Analysis of Tissue Thrombin Expression in the Human Atria

Keiichi Ito[1]*, Taro Date[1], Masahiro Ikegami[2], Kenichi Hongo[1], Masami Fujisaki[1], Daisuke Katoh[1], Takuya Yoshino[1], Ryuko Anzawa[1], Tomohisa Nagoshi[1], Seigo Yamashita[1], Keiichi Inada[1], Seiichiro Matsuo[1], Teiichi Yamane[1], Michihiro Yoshimura[1]

1 Division of Cardiology, Department of Internal Medicine, The Jikei University School of Medicine, Minato-ku, Tokyo, Japan, **2** Department of Pathology, The Jikei University School of Medicine, Minato-ku, Tokyo, Japan

Abstract

Objective: Thrombin, the final coagulation product of the coagulation cascade, has been demonstrated to have many physiological effects, including pro-fibrotic actions via protease-activated receptor (PAR)-1. Recent investigations have demonstrated that activation of the cardiac local coagulation system was associated with atrial fibrillation. However, the distribution of thrombin in the heart, especially difference between the atria and the ventricle, remains to be clarified. We herein investigated the expression of thrombin and other related proteins, as well as tissue fibrosis, in the human left atria and left ventricle.

Methods: We examined the expression of thrombin and other related molecules in the autopsied hearts of patients with and without atrial fibrillation. An immunohistochemical analysis was performed in the left atria and the left ventricle.

Results: The thrombin was immunohistologically detected in both the left atria and the left ventricles. Other than in the myocardium, the expression of thrombin was observed in the endocardium and the subendocardium of the left atrium. Thrombin was more highly expressed in the left atrium compared to the left ventricle, which was concomitant with more tissue fibrosis and inflammation, as detected by CD68 expression, in the left atrium. We also confirmed the expression of prothrombin in the left atrium. The expression of PAR-1 was observed in the endocardium, subendocardium and myocardium in the left atrium. In patients with atrial fibrillation, strong thrombin expression was observed in the left atrium.

Conclusions: The strong expression levels of thrombin, prothrombin and PAR-1 were demonstrated in the atrial tissues of human autopsied hearts.

Citation: Ito K, Date T, Ikegami M, Hongo K, Fujisaki M, et al. (2013) An Immunohistochemical Analysis of Tissue Thrombin Expression in the Human Atria. PLoS ONE 8(6): e65817. doi:10.1371/journal.pone.0065817

Editor: Rajasingh Johnson, University of Kansas Medical Center, United States of America

Received February 15, 2013; **Accepted** April 28, 2013; **Published** June 13, 2013

Funding: The authors have no support or funding to report.

Competing Interests: The authors have declared that no competing interests exist.

* E-mail: keke-ito@jikei.ac.jp

Introduction

Thrombin, the final coagulation product of the coagulation cascade, plays various physiological roles, including pro-fibrotic actions via protease-activated receptor (PAR)-1, PAR-2 and PAR-4 [1]. PAR-1 is also involved in vessel wound healing and revascularization [2], platelet procoagulant activity [3] and gastric contraction [4]. In lung tissue, the induction of myofibroblasts occurs primarily via the actions of PAR-1 [5], [6], and a recent study demonstrated the importance of PAR-1 in the pathogenesis of fibrosis in cardiac fibroblasts [7].

Recent clinical investigations have demonstrated that the local coagulation system in the heart is activated in patients with atrial fibrillation [8], [9], [10]. Thrombin is known to exist in several tissues, such as the endothelium [11] and fibroblasts [12]. However, there have been few reports that have immunohistologically analyzed the distribution of thrombin in the heart, or the roles of tissue thrombin in the inflammatory process and fibrosis, which is a substrate of atrial tachyarrhythmias [13].

In this study, we investigated the expression of thrombin and other related molecules in the left atrium and left ventricle of patients with and without atrial fibrillation.

Methods

Informed consent have been obtained and all clinical investigation have been conducted according to the principles expressed in the Declaration of Helsinki. We have obtained approval from the Ethics Committee of Jikei University School of Medicine. We did not conduct research outside of our country of residence. The full names of our ethics committees and the institutions/hospitals we are associated with are "the Ethics Committee of Jikei University School of Medicine". Participants have provided their written informed consent to participate in this study. An immunohistochemical analysis of the expression and localization of thrombin, prothrombin, PAR-1 and CD68 was performed in 7 patients (patient 1: a 71-year-old male who died of ischemic colitis and septic shock and had no history of atrial fibrillation, patient 2:

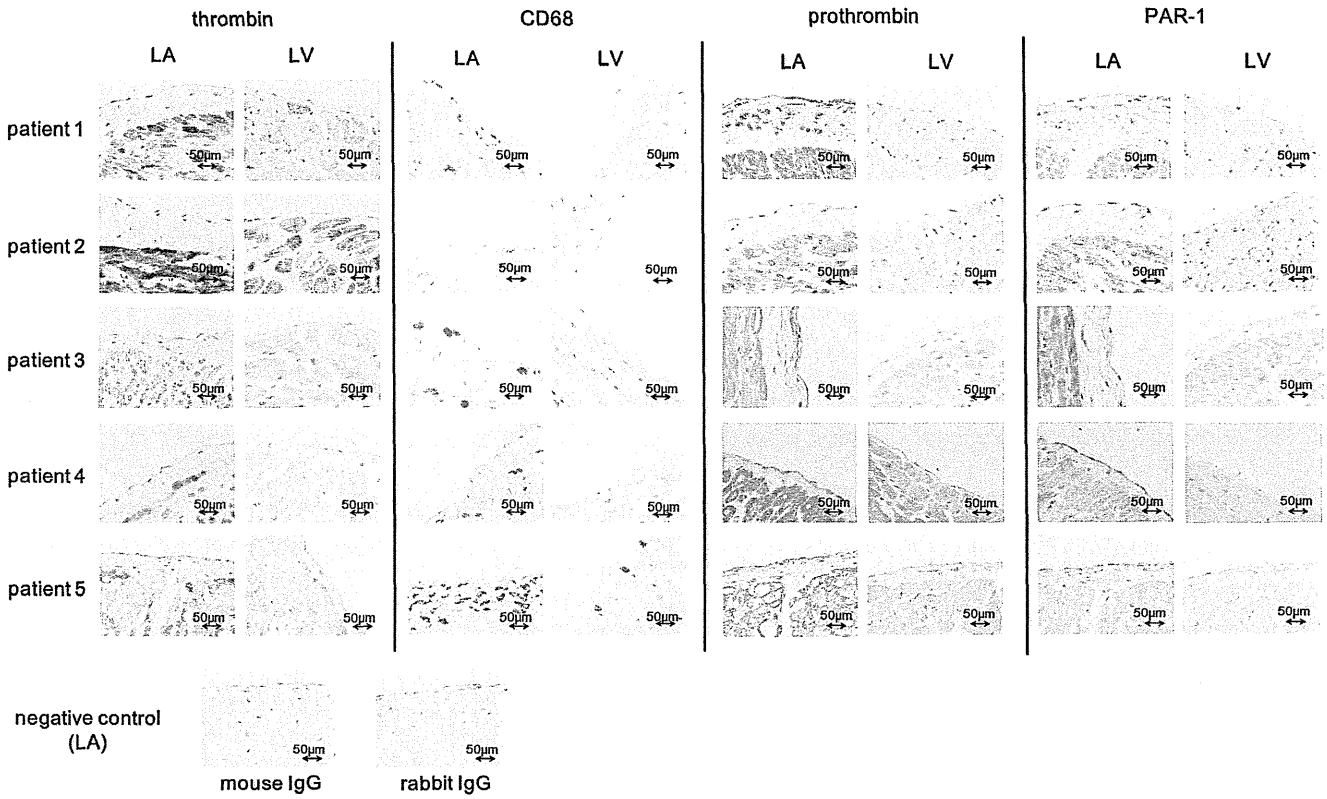

Figure 1. The results of the immunohistochemical analysis of the expression of thrombin, CD68, prothrombin and PAR-1 in the LA and the LV around the endocardium obtained from human autopsied hearts of patients without any history of AF (×40). The expression of thrombin, CD68, prothrombin and PAR-1 was evident in the LA around the thick subendocardial space of the LA. LA: left atrium, LV: left ventricle.
doi:10.1371/journal.pone.0065817.g001

an 85-year-old male who died of hepatocellular carcinoma caused by hepatitis C virus infection and had no history of atrial fibrillation, patient 3: a 67-year-old male who died of chronic lymphocytic lymphoma and had no history of atrial fibrillation, patient 4: a 77-year-old male who died of pneumonia and had no history of atrial fibrillation, patient 5: a 50-year-old male who died of acute myeloid leukemia and had no history of atrial fibrillation, patient 6: a 75-year-old male who died of intrahepatic bile duct carcinoma who had a history of paroxysmal atrial fibrillation, patient 7: a 69-year-old male who died of pneumonia and had a history of ventricular tachycardia and atrial fibrillation).

Sections obtained from formalin-fixed, paraffin-embedded specimens were stained with hematoxylin and eosin and Masson trichrome stain. For the immunohistochemical analyses, sections were deparaffinized and digested with 0.05% subtilisin. The inactivation of endogenous peroxidase activity was performed by incubation in 3% H_2O_2 in methanol for 30 minutes. After several washes in phosphate buffered saline (PBS), the slides were heated in a microwave oven at 121°C for antigen retrieval. After being cooled at room temperature and washed with PBS, the sections were incubated with blocking solution for one hour at room temperature. Then, after PBS washing, the tissues were bordered with a pap-pen. The sections were incubated with mouse monoclonal antibodies against thrombin (Santa Cruz, Delaware Avenue, CA), PAR-1 (Santa Cruz, Delaware Avenue, CA), PAR-2 (Santa Cruz, Delaware Avenue, CA), PAR-4 (Santa Cruz, Delaware Avenue, CA), alpha-smooth muscle actin (αSMA) (Dako, Carpenteria, CA) and CD68 (Dako, Carpenteria, CA), or with rabbit polyclonal antibodies against prothrombin (Bioworld Technology, England) and PAR-3 (Santa Cruz, Delaware Avenue, CA) for 30 minutes at room temperature following standard protocols. The antigen retrieval was changed based on the primary antibodies used. For the thrombin and PAR-4 antibodies, antigen retrieval was performed in citric acid buffer (pH 6.0, 0.01 M) for 10 minutes. For the PAR-1 antibody, antigen retrieval was performed in target retrieval solution with a high pH (Dako, Carpenteria, CA) for 10 minutes. For the prothrombin and CD68 antibodies, antigen retrieval was carried out in protease for one minute. The sections were visualized using Nikon Eclipse 80i with a Nikon Digital Camera DXM 1200. CD68-positive cells were enumerated using a ×40 objective lens as described previously [14]. The fields were chosen at random by blind and sequential movement of the mechanical stage. Very large vessels were excluded from the counts. At least 20 random fields were counted. The immunohistochemical staining was scored subjectively on a semi-quantitative scale of 0–4 (0 = no staining, 1 = weak staining, 2 = moderate staining, 3 = strong staining, 4 = intense staining), as described previously [15]. Statistical comparisons between groups were performed using the Wilcoxon test. All statistical analyses were performed using the SPSS software program (version 21, SPSS Japan Inc., Tokyo, Japan), and differences were considered to be statistically significant for values of $p<0.05$.

Results

The immunohistochemical analysis demonstrated the expression of tissue thrombin to be observed in the endocardium, subendocardium and myocardium in the left atrium (LA) and the

left ventricle (LV) in all five patients without a history of AF (Figure 1). In the myocardium of the LA, as in the endocardium, the thrombin expression levels were higher in the LA compared to the LV (Figure 1, averaged scores: 2.4 vs. 0.8 in the endocardium/subendocardium, 2.6 vs. 1.0 in the myocardium, $p<0.05$). The CD68 positivity was also more prominent in the endocardium/subendocardium of the LA than the LV (Figure 1, 5.9/high power field (LA) vs. 3.7/high power field (LV), $p<0.05$). Masson trichrome staining showed that more fibrosis was present in the subendocardial space and interstitium of the LA compared to that of the LV, which was concomitant with the thrombin expression (Figure 2).

We also investigated the expression of prothrombin and PAR-1 in the LA and LV, and found that they were both detected in the endocardium, subendocardium and myocardium of the LA in all of the studied patients without a history of AF (Figure 1). The semi-quantitative scores of the prothrombin expression were higher in the LA compared to the LV (Figure 1, averaged scores: 3.4 vs. 1.0 in the endocardium/subendocardium, 2.8 vs. 1.2 in the myocardium, $p<0.05$). The PAR-1 expression was also stronger in the LA compared to the LV (Figure 1, averaged scores: 2.4 vs. 0.8 in the endocardium/subendocardium, 2.2 vs. 0.8 in the myocardium, $p<0.05$). We also examined the expression levels of these molecules in tissue specimens from other organs, and significant thrombin, prothrombin and PAR-1 expression was detected in the liver, which also served as a positive control for prothrombin expression, and in the pulmonary artery wall (Figure 3).

We next examined the expression of thrombin and other related molecules in patients with atrial fibrillation. An immunohistological analysis of the LA from patients with AF showed strong thrombin expression in the myocardium and thick, fibrotic subendocardial space of the LA (averaged scores: 3.0 in the endocardium/subendocardium, 3.5 in the myocardium) (Figure 4) as well as strong prothrombin expression (averaged scores: 3.5 in the endocardium/subendocardium and 4 in the myocardium) and PAR-1 expression (averaged scores: 3.5 in the endocardium/subendocardium and 2.5 in the myocardium) (Figure 4). The tissue thrombin detected in the subendocardial space of LA was co-localized with CD68-positive areas, indicating that some of the thrombin was derived from macrophages (Figure 5). PAR-4, another important thrombin receptor, was positively stained in the LA (Figure 6), whereas PAR-2 and PAR-3 expression were barely observed in the LA (data not shown). Of note, some of the tissue thrombin in the subendocardial space of the LA was co-localized with the αSMA expression, which is a marker of the profibrogenic myofibroblast phenotype (Figure 6). These findings suggest that thrombin plays an important role in promoting atrial fibrosis through the conversion of cardiac fibroblasts to a profibrogenic phenotype.

Discussion

The present study demonstrated, for the first time, that the prominent local expression of thrombin can be detected immunohistochemically in the human atrium, and that this expression was partially associated with the CD68 expression and tissue fibrosis.

Recent data suggest the possible involvement of the coagulation system in various fibrotic diseases, including pulmonary fibrosis. The process of activating the coagulation system depends on the actions of thrombin. There are four types of thrombin receptors: PAR-1, PAR-2, PAR-3 and PAR-4. These thrombin receptors are members of the G-protein-coupled receptor (GPCR) family [16]. Previous studies have reported that the various physiological roles of thrombin are mediated through the actions of PAR-1 in cardiac fibroblasts[7]. Thrombin interacts with PAR-1, PAR-2 and PAR-4, and cleaves their N-terminus to unveil the pentapeptide [16]. The existence of thrombin in several tissues has been suggested in previous reports [11], [12], [16]. Akar et al. demonstrated that activation of the cardiac local coagulation system was associated with paroxysmal attacks of atrial fibrillation [9]. These previous investigations prompted us to immunohistologically analyze the expression levels of thrombin and related molecules in the human heart. In the present study, we investigated the expression levels of thrombin and prothrombin in the LA, in which we were able to detect both thrombin and prothrombin in the endocardium, subendocardium and myocardium. In addition, our data provide evidence that PAR-1 and PAR-4 are expressed in the atrial tissue, thus suggesting that thrombin plays an important functional role in the atria. Notably, the co-localization of the CD68-stained areas with the expression of prothrombin and thrombin revealed that the source of thrombin could be invasive macrophages present in the atrium. Yamashita et al. demonstrated active adhesion and recruitment of macrophages across the endocardium in human fibrillating atria, with local inflammatory responses around the endocardial regions [17]. Our observations prompted us to hypothesize that the inflammation and the subsequent fibrotic changes induced by invasive macrophages around the atrial endocardium may be at least partly mediated by thrombin. The present study demonstrated that increased thrombin expression was observed in the rich fibrotic areas, especially in the LAs of the patients with a history of AF. A recent investigation demonstrated that thrombin induced the conversion of cardiac fibroblasts to a profibrogenic myofibroblast phenotype, as indicated by αSMA expression, via PAR-1 activation and an increase in collagen synthesis [7]. Our present observations demonstrated that αSMA

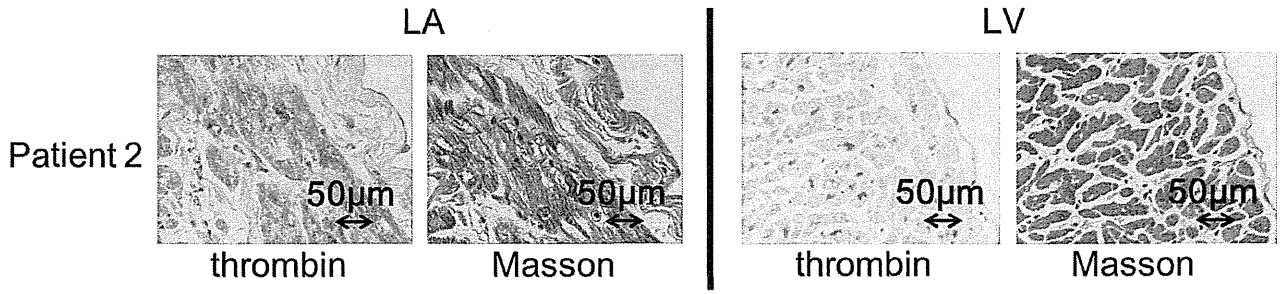

Figure 2. The results of the immunohistochemical analysis of the thrombin expression and Masson trichrome staining in the serial sections obtained from patient (×10). LA: left atrium, LV: left ventricle. A larger fibrotic area was observed in the LA than in the LV.
doi:10.1371/journal.pone.0065817.g002

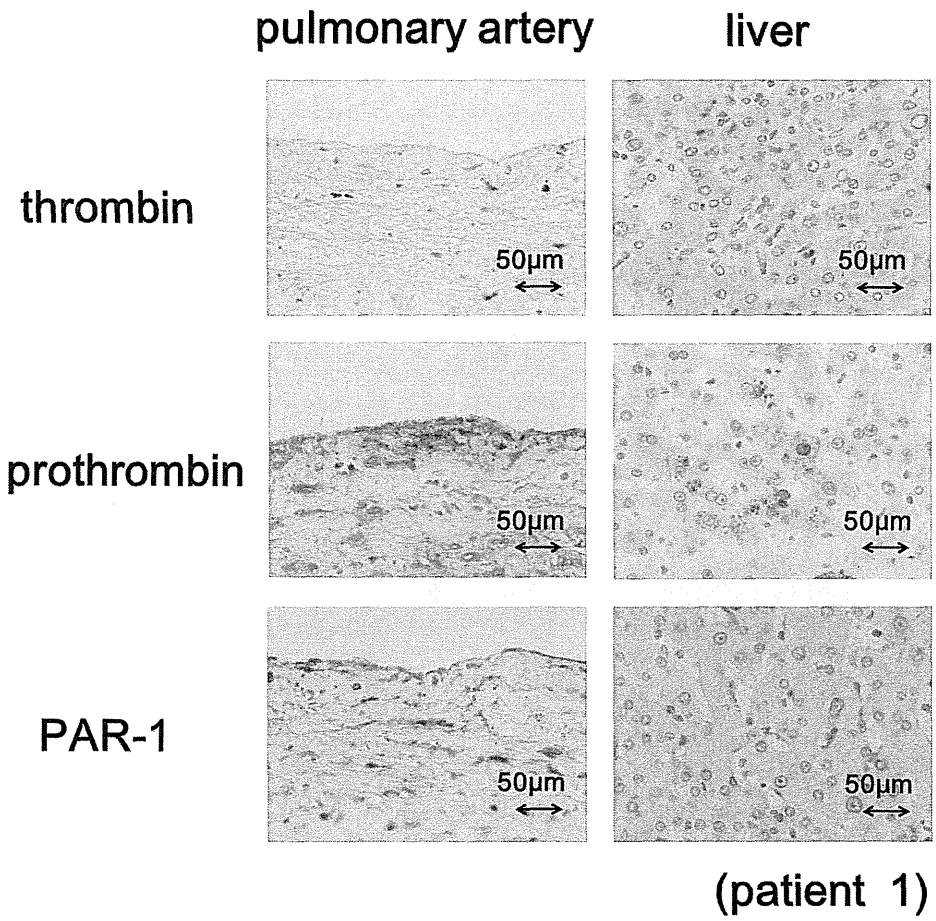

Figure 3. The results of an immunohistochemical analysis of the expression of thrombin, prothrombin and PAR-1 in the pulmonary artery and liver of human autopsied tissues. The expression of thrombin, prothrombin and PAR-1 was confirmed in the liver (positive control). Thrombin was sparsely stained, and both prothrombin and PAR-1 were distinctly detected in the pulmonary artery.
doi:10.1371/journal.pone.0065817.g003

was co-localized with the thrombin expression, especially in the sub-endocardial region. Taken together, these findings suggest that tissue thrombin in the atria may promote atrial fibrosis, which can cause atrial tachyarrhythmias. Recent findings have shown that PAR-1 and PAR-4 activation both contribute to cardiac remodeling and influence cardiac inflammation [18], [19]. PAR-1 and PAR-4 signaling might also be related to tissue fibrosis in the atria. The precise reason why increased thrombin expression was observed in the LA of the patients with a history of AF remains to be determined. However, it was reported that oxidant stress may enhance the thrombin expression in brain endothelial cells [20]. It is therefore possible that elevated oxidative stress, which is associated with the pathogenesis of AF [21], may lead to the upregulation of thrombin expression. Further studies are required to determine the physiological and pathological roles of tissue thrombin.

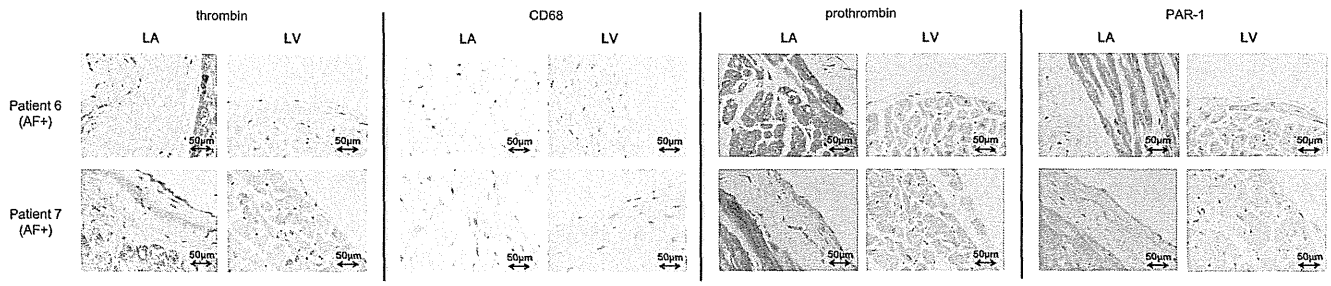

Figure 4. The results of an immunohistochemical analysis of the expression of thrombin, CD68, prothrombin and PAR-1 in the LA of autopsied hearts from patients with AF (AF(+): patient 6 and patient 7) (×40). Thrombin was highly expressed in the myofibers, as well as the endocardium and subendocardium. CD68 positivity was noted in the LA, but was comparable to that in the patients without AF. Prothrombin and PAR-1 were highly detected in these sections in the LA. LA: left atrium.
doi:10.1371/journal.pone.0065817.g004

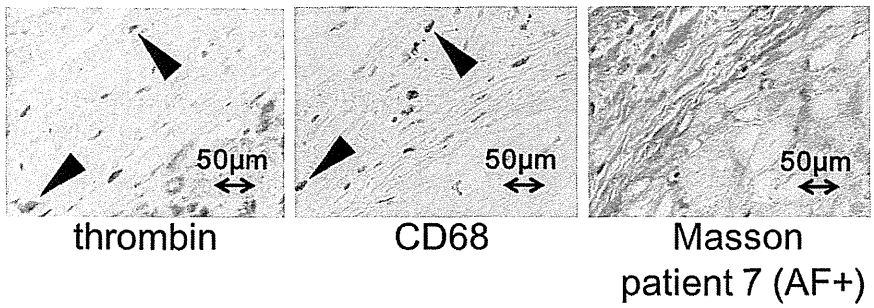

Figure 5. The results of an immunohistochemical analysis of the expression of thrombin and CD68, as well as Masson trichrome staining, in the serial sections of the LA from the autopsied heart of a patient with AF (patient 7). Notably, the co-localization of the CD68-stained areas with the thrombin expression was revealed, indicating that the source of thrombin could be invasive macrophages present in the atria. A thick fibrotic sub-endocardial layer was present in the LA, as indicated by Masson trichrome staining. Masson: Masson trichrome staining, LA: left atrium, AF: atrial fibrillation.
doi:10.1371/journal.pone.0065817.g005

The present study demonstrated the staining for thrombin in the human atria tissue. Two mechanisms; the expression and the clearance, were estimated to underlie the staining of thrombin. In the endothelium, thrombin co-localizes with thrombomodulin, and they are both internalized and removed from the circulation by the endothelium [11]. The clearance of thrombin from the circulation occurs via two pathways [22]. One pathway involves the endothelial route discussed above, and the other involves its removal by the liver. Antithrombin III binds to thrombin, and the thrombin-antithrombin III complex is removed by the liver [22]. Therefore, the endothelium and liver both clear thrombin from the circulation. Although the presence of the tissue thrombin outside of the endothelium has been reported in chick embryonic fibroblasts [12], the role of tissue thrombin has not been elucidated [12]. The presence of prothrombin in tissues has also been reported in a previous study [23]. Functionally intact prothrombin

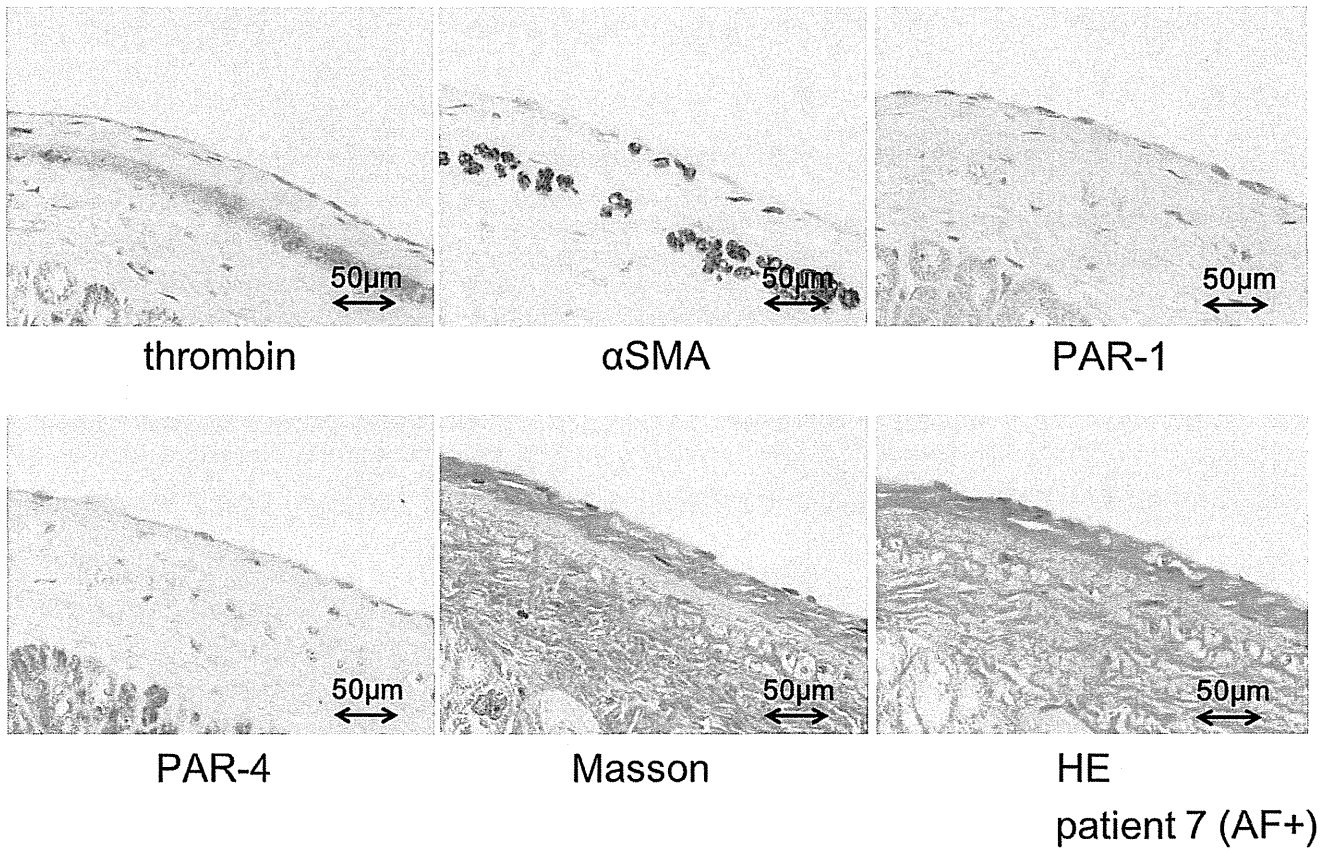

Figure 6. The results of an immunohistochemical analysis of the expression of thrombin, αSMA, PAR-1 and PAR-4, as well as Masson trichrome staining and HE staining, in the serial sections of the LA from the autopsied heart of a patient with AF (patient 7). Co-localization of the αSMA-stained areas with the thrombin expression was noted in the fibrotic sub-endocardial layer of the LA, as determined by Masson trichrome staining. Masson: Masson trichrome staining, LA: left atrium, AF: atrial fibrillation.
doi:10.1371/journal.pone.0065817.g006

is widely distributed among various tissues, including the myocardium; however, the physiological significance of tissue prothrombin remains unclear [23]. Although the thrombin of the atrial tissue may be derived from the cleared thrombin from the circulation across the endocardium and the vascular endothelium, the possibility of local production of thrombin in the atria cannot be ruled out.

In conclusion, the expression of thrombin in the atrial tissues of human autopsied hearts was demonstrated. Further research is needed to determine the physiological and pathological roles of atrial tissue thrombin.

Acknowledgments

We thank Dr. Brian Quinn (Japan Medical Communication) for his kind advice regarding the use of the English language. We also thank to Dr. Shun Sato (Department of Pathology, The Jikei University School of Medicine) for his valuable contributions to the immunohistochemical analyses.

Author Contributions

Conceived and designed the experiments: K. Ito TD MI KH MY. Performed the experiments: K. Ito TD MI KH MY. Analyzed the data: MF DK T. Yoshino RA TN SY K. Inada SM T. Yamane. Contributed reagents/materials/analysis tools: MF DK T. Yoshino RA TN SY K. Inada SM T. Yamane. Wrote the paper: K. Ito TD MI KH MY.

References

1. Ruf W, Dorfuleutner A, Riewald (2003) Specificity of coagulation factor signaling. J Thrombo Hemost 1: 1495–1503.
2. Carney DH, Mann R, Redin WR, Pernia SD, Berry D, et al. (1992) Enhancement of incisional wound-healing and neovascularisation in normal rats by thrombin and synthetic thrombin receptor activating peptides. J Clin Invest 89: 1469–1477.
3. Anderson H, Greenberg DL, Fujikawa K, Xu WF, Chung DW, et al. (1999) Protease-activated receptor 1 is the primary mediator of thrombin-stimulated platelet procoagulant activity. Proc Natl Acad Sci USA 96: 11189–11193.
4. Hollenberg MD, Yang SG, Laniyonu AA, Moore GJ, Saiffedine M (1992) Action of thrombin receptor polypeptide in gastric smooth muscle-Identification of a core pentapeptide retaining full thrombin-mimetic intrinsic activity. Molecular Pharmacology 42: 186–191.
5. Bogatkevich GS, Ludwicka-Bradley A, Silver RM (2009) Dabigatran, a direct thrombin inhibitor, demonstrates antifibrotic effects on lung fibroblasts. Arthritis Rheum 60: 3455–64.
6. Cooper DM, Pechkovsky DV, Hackett TL, Knight DA, Granville DJ (2011) Granzyme K activates protease-activated receptor-1. PloS One 6: e21484.
7. Aaron NS, Paul AI (2012) Defining the cellular repertorie of GPCRs identifies a progibrotic role for the most highly expressed receptor, protease-activated receptor 1, in cardiac fibroblasts. The FASEB Journal 26: 4540–7.
8. Choudhury A, Lip GY (2003) Atrial fibrillation and the hypercoagulable state: from basic science to clinical practice. Pathophysiol Haemost Thromb. 33: 282–9.
9. Akar JG, Jeske W, Wilber DJ (2008) Acute onset human atrial fibrillation is associated with local cardiac platelet activation and endothelial dysfunction. J Am Coll Cardiol. 51: 1790–3.
10. Yan GX, Park TH, Corr PB (1995) Activation of thrombin receptor increases intracellular Na+ during myocardial ischemia. Am J Physiol. 268: H1740–8.
11. Horvat R, Palade GE (1993) Thrombomodulin and thrombin localization on the vascular endocardium; their internalization and transcytosis by plasmalemmal vesicles. Eur J Cell Biol 61: 293–313.
12. Zetter BR, Chen LB, Buchanan JM (1977) Binding and internalization of thrombin by normal and transformed chick cells. Proc Natl Acad Sci USA 74: 596–600.
13. Xu J, Cui G, Esmailian F, Plunkett M, Marelli D, et al. (2004) Atrial extracellular matrix remodeling and the maintenance of atrial fibrillation. Circulation 109: 363–368.
14. Azzawi M, Hasleton PS, Kan SW, Hillier VF, Quigley A, et al. (1997) Distribution of myocardial macrophages in the normal human heart. J Anat 191: 417–23.
15. Au CL, Rogers PA (1993) Immunohistochemical staining of von Willebrand factor in human endometrium during normal menstrual cycle. Hum Reprod. 8: 17–23.
16. Macfarlane SR, Seatter MJ, Kanke N, Hunter GD, Plevin R (2001) Proteinase-Activated Receptors. Pharmacol Rev 53: 245–282.
17. Yamashita T, Sekiguchi A, Iwasaki YK, Date T, Sagara K, et al. (2010) Recruitment of immune cells across atrial endocardium in human atrial fibrillation. Circ J 74: 262–70.
18. Sabri A, Guo J, Elouardighi H, Darrow AL, Andrade-Gordon P, et al. (2003) Mechanisms of protease-activated receptor-4 actions in cardiomyocytes. Role of Src tyrosine kinase. J Biol Chem. 278: 11714–20.
19. Pawlinski R, Tencati M, Hampton CR, Shishido T, Bullard TA, et al. (2007) Protease-activated receptor-1 contributes to cardiac remodeling and hypertrophy. Circulation. 116: 2298–306.
20. Yin X, Wright J, Wall T, Grammas P (2010) Brain endothelial cells synthesize neurotoxic thrombin in Alzheimer's disease. Am J Pathol 176: 1600–6.
21. Shiroshita-Takeshita A, Schram G, Lavoie J, Nattel S (2004) Effect of simvastatin and antioxidant vitamins on atrial fibrillation promotion by atrial-tachycardia remodeling in dogs. Circulation. 110: 2313–9.
22. Lollar P, Owen WG (1980) Clearance of thrombin from circulation in rabbits by hi-affinity binding sites on endothelium. J Clin Invest 66: 1222–30.
23. McBane RD 2nd, Miller RS, Hassinger NL, Chesebro JH, Nemerson Y, et al. (1997) Tissue Prothrombin. Universal distribution in smooth muscle. Arterioscler Thromb Vasc Biol 17: 2430–6.

Heart Vessels (2013) 28:646–657
DOI 10.1007/s00380-012-0311-0

ORIGINAL ARTICLE

Atrial natriuretic peptide exerts protective action against angiotensin II-induced cardiac remodeling by attenuating inflammation via endothelin-1/endothelin receptor A cascade

Shuichi Fujita · Naoshi Shimojo · Fumio Terasaki · Kaoru Otsuka · Noriko Hosotani · Yuka Kohda · Takao Tanaka · Tomohiro Nishioka · Toshimichi Yoshida · Michiaki Hiroe · Yasushi Kitaura · Nobukazu Ishizaka · Kyoko Imanaka-Yoshida

Received: 29 June 2012 / Accepted: 30 November 2012 / Published online: 1 January 2013

Abstract We aimed to investigate whether atrial natriuretic peptide (ANP) attenuates angiotensin II (Ang II)-induced myocardial remodeling and to clarify the possible molecular mechanisms involved. Thirty-five 8-week-old male Wistar–Kyoto rats were divided into control, Ang II, Ang II + ANP, and ANP groups. The Ang II and Ang II + ANP rats received 1 μg/kg/min Ang II for 14 days. The Ang II + ANP and ANP rats also received 0.1 μg/kg/min ANP intravenously. The Ang II and Ang II + ANP rats showed comparable blood pressure. Left ventricular fractional shortening and ejection fraction were lower in the Ang II rats than in controls; these indices were higher ($P < 0.001$) in the Ang II + ANP rats than in the Ang II rats. In the Ang II rats, the peak velocity of mitral early inflow and its ratio to atrial contraction-related peak flow velocity were lower, and the deceleration time of mitral early inflow was significantly prolonged; these changes were decreased by ANP. Percent fibrosis was higher ($P < 0.001$) and average myocyte diameters greater ($P < 0.01$) in the Ang II rats than in controls. ANP decreased both myocardial fibrosis ($P < 0.01$) and myocyte hypertrophy ($P < 0.01$). Macrophage infiltration, expression of mRNA levels of collagen types I and III, monocyte chemotactic protein-1, and a profibrotic/proinflammatory molecule, tenascin-C (TN-C) were increased in the Ang II rats; ANP significantly decreased these changes. In vitro, Ang II increased expression of TN-C and endothelin-1 (ET-1) in cardiac fibroblasts, which were reduced by ANP. ET-1 upregulated TN-C expression via endothelin type A receptor. These results suggest that ANP may protect the heart from Ang II-induced remodeling by attenuating inflammation, at least partly through endothelin 1/endothelin receptor A cascade.

Keywords ANP · Cardiac remodeling · Tenascin-C · Inflammation · Endothelin-1

S. Fujita · N. Shimojo · F. Terasaki · K. Otsuka · Y. Kitaura · N. Ishizaka (✉)
Department of Cardiology, Osaka Medical College, 2-7 Daigaku-machi, Takatsuki, Osaka 569-8686, Japan
e-mail: ishizaka@poh.osaka-med.ac.jp

N. Shimojo · T. Nishioka · T. Yoshida · K. Imanaka-Yoshida (✉)
Department of Pathology and Matrix Biology, Mie University Graduate School of Medicine, 2-174 Edobashi, Tsu, Mie 514-8507, Japan
e-mail: kyimanaka@gmail.com

N. Shimojo · T. Yoshida · K. Imanaka-Yoshida
Mie University Research Center for Matrix Biology, 2-174 Edobashi, Tsu, Mie 514-8507, Japan

N. Hosotani · Y. Kohda
Laboratory of Pharmacotherapy, Osaka University of Pharmaceutical Sciences, 4-20-1 Nasahara, Takatsuki, Osaka 569-1094, Japan

T. Tanaka
Department of Nursing Science, Baika Women's University, 2-19-5 Shukunosho, Ibaraki, Osaka 567-8578, Japan

M. Hiroe
Department of Cardiology, National Center of Global Health and Medicine, 1-2-1Toyama, Shinjuku-ku, Tokyo 162-8655, Japan

Introduction

Atrial natriuretic peptide (ANP) was originally identified as a diuretic/natriuretic and vasodilating hormone released by the heart in response to myocardial stretch and overload. Recent reports have demonstrated that ANP exerts various beneficial effects on the heart [1–3], For example. ANP

suppresses the renin-angiotensin-aldosterone system (RAAS), endothelin synthesis, and sympathetic nerve activity [4], whereas it enhances adiponectin production and regulates cell growth and apoptosis (reviewed in [5, 6]), as a circulating hormone as well as a local autocrine and/or paracrine factor. Indeed, ANP exhibits therapeutic efficacy against chronic heart failure [7–9], acute heart failure [10–13], and acute myocardial infarction [14–17] in humans as well as rat models of acute myocardial infarction–reperfusion [18] and autoimmune myocarditis [19]. However, the detailed molecular mechanisms of these cardioprotective functions remain uncertain.

Left ventricular (LV) remodeling is an important factor related to the prognosis of heart disease. Histological features of LV remodeling include interstitial fibrosis and myocyte hypertrophy. Enhanced myocardial stiffness caused by increased interstitial fibrosis is known to lead to diastolic heart failure. Recently, increasing attention has been paid to the fact that RAAS overactivation-mediated inflammation plays a significant role in the development of cardiac fibrosis during ventricular remodeling [20–23]. Fibrotic lesions are formed via a multistep process of synthesis and degradation of various extracellular matrix molecules, including tenascin-C (TN-C). TN-C is an extracellular glycoprotein that is weakly expressed in healthy adult hearts, but it is transiently upregulated in association with tissue injury and inflammation [24–30]. This specific expression pattern makes TN-C a valuable marker for inflammatory disease activity [25, 27]. Using a mouse model, we previously reported that TN-C may be involved in the progression of hypertensive myocardial fibrosis and that elevated TN-C expression may be a marker for active progression of fibrosis in the heart [28]. Furthermore, TN-C has diverse biological functions and is considered to be a key molecule during the progression of inflammation and fibrosis (reviewed in [31, 32]). We investigated whether ANP attenuates cardiac fibrosis in a rat model of Ang II-induced ventricular remodeling and the molecular mechanism involved, especially focusing on TN-C. Cardiac function, histological changes, and expression of molecules related to fibrosis and inflammation, which include collagen type I, collagen type III, TN-C, monocyte chemotactic protein-1 (MCP-1), and endothelin-1 (ET-1) were examined in the heart of model rats treated with Ang II with or without ANP. Furthermore, the direct effects of ANP on TN-C synthesis and the signaling pathways involved were studied in cultured cardiac fibroblasts.

Materials and methods

Animal experiments were performed in accordance with the *Guide for the Care and Use of Laboratory Animals* published by the US National Institutes of Health (publication no. 85-23, revised 1996), and the study was approved by our Institutional Animal Research Committee. Experiments were performed on 8-week-old male Wistar–Kyoto rats that weighed 250–280 g before study initiation. The rats were fed a standard rat-chow diet and had free access to tap water. Thirty-five rats were randomly divided into four treatment groups (control, $n = 10$; Ang II, $n = 10$; Ang II + ANP, $n = 10$, ANP, $n = 5$). All rats were anesthetized with 3 % isoflurane on a volume-cycled ventilator (Univentor; Bio Research Center, Nagoya, Japan) for small animals. In Ang II and Ang II + ANP groups, a midline incision was made in the lumbar region for insertion of osmotic mini-pumps (model 2002; ALZET, Palo Alto, CA, USA; mean filling volume, 0.234 ml) filled with Ang II (Peptide Institute, Osaka, Japan), which was infused at 1 μg/kg/min for 14 days. The dose used in this study was determined on the basis of preliminary experiments. For the administration of saline or ANP, control, Ang II + ANP, and ANP groups bearing the mini-pump were fitted with a fluid-delivery infusion pump (10 ml Infu-disk; MED-e-CELL, San Diego, CA, USA) attached to the back. These external infusion pumps were filled with saline or carperitide, a recombinant α-human ANP (Daiichi-Sankyo Pharmaceutical, NY, USA), dissolved in distilled water and released at 0.1 μg/kg/min for 14 days. The pump was connected to the right or left jugular vein by a small polyethylene catheter. The rats were weighed on days 0, 3, 6, 10, and 14, and systolic blood pressure and heart rate were measured using a tail-cuff method without anesthesia on the same days. On day 14, the rats were deeply anesthetized with isoflurane and euthanized. The hearts were dissected and weighed, and a part of the ventricle was separated from the heart, frozen in RNAlater (Ambion, Huntington, UK), and stored at −80 °C until use.

Echocardiographic measures of cardiac function

LV function was assessed using a two-dimensional guided M-mode ultrasound system (VIVID7; GE Medical Systems, Tokyo, Japan). Images of the short-axis view of the left ventricle at the level of the papillary muscle were recorded to assess cardiac function. The end-diastolic LV dimension (LVDd) and end-systolic LV dimension (LVDs) were measured directly by echocardiography. The LV fractional shortening (FS) and LV ejection fraction (EF) were calculated as percentages from the LVDd and LVDs values. The LV diastolic function was evaluated by recording the pulse-wave Doppler spectra of transmitral flow. The peak velocity of mitral early inflow (*E*), its ratio to atrial contraction-related flow peak velocity (*E/A*), and the deceleration time of mitral early inflow (DcT) were also

measured. Echocardiography was performed on the 14th day after study initiation in all rats.

Histological analysis

Histological analysis was performed on five hearts from each group. The left ventricle was removed, fixed in 4 % paraformaldehyde, and embedded in paraffin. Three-micrometer-thick sections were prepared and stained with hematoxylin–eosin for evaluation of myocyte hypertrophy and with Sirius Red for evaluation of myocardial fibrosis. To determine the average myocyte size, the shortest transverse diameter was measured in 50 transverse sections per heart (×200 magnification), which contained the cross section of a myocyte with its nucleus. To determine the percent area of myocardial interstitial and perivascular fibrosis, the Scion imaging system (Scion, Frederick, MD, USA) was used as described previously [28]. To evaluate TN-C expression and the number of macrophages in the myocardium, we performed immunohistochemistry as described previously [33]. In brief, a mouse monoclonal antibody for TN-C (4F10TT; IBL, Gunma, Japan; 1:100 dilution) and a mouse monoclonal antibody against the macrophage marker cluster of differentiation 68 (CD68; DAKO Japan, Tokyo, Japan; 1:100 dilution) were used. Immunoreactivity was evaluated using the avidin–biotin–peroxidase complex method (ScyTek Laboratories, Logan, UT, USA). The reactions were visualized using diaminobenzidine, and nuclei were counterstained with hematoxylin. Quantitative analysis of tissue macrophages was performed using the CD68 antibody stain. For each-specimen, three randomly selected photomicrographs (×400 magnification) of the anterior, lateral, and posterior ventricular walls, as well as the interventricular septum, were examined (12 fields/specimen). The numbers of CD68-positive cells were counted in each region and expressed as the number of inflammatory cells per unit area (1 mm^2).

Immunofluorescence double labeling was applied to colocalize TN-C, and either α-smooth muscle actin (SMA)-positive cells or macrophages. Anti-α-SMA mouse monoclonal primary antibodies (Thermo Fisher Scientific, Yokohama, Japan; 1:100 dilution) were used for the detection of α-SMA-positive cells, and anti-CD68 mouse monoclonal primary antibodies (DAKO Japan; 1:100 dilution) were used for detection of macrophages. Biotinylated antimouse immunoglobulins (EPOS; Dako Japan; 1:250 dilution) were then used as part of the enhanced polymer one-step staining system, followed by incubation in streptavidin labeled with Alexa 448 (Molecular Probes, Eugene, OR, USA; 1:300 dilution). For detection of TN-C, anti-TN-C polyclonal rabbit antibody [33], and goat anti-rabbit immunoglobulins labeled with Alexa 555 (Molecular Probes; 1:300 dilution) were used. Fluoromount (Diagnostic BioSystem, Pleasanton, CA, USA) was used to mount stained sections on coverslips. Laser scanning confocal fluorescence microscopy combined with differential interference contrast imaging was performed using LSM 510 META Ver. 3.2 (Zeiss, Göttingen, Germany). Brightness and contrast adjustments along with necessary cropping were performed using Photoshop Elements 8.0 (Adobe, San José, CA, USA).

Real-time reverse transcription–polymerase chain reaction (real-time RT-PCR)

Total RNA was isolated from five hearts from each group and real-time RT-PCR performed to measure the mRNA expression levels of collagen type I, collagen type III, TN-C, MCP-1, ET-1, and glyceraldehyde-3-phosphate dehydrogenase (GAPDH). Quantitative PCR was performed using a Light Cycler (LightCycler FastStart DNA Master PLUS SYBR Green I; Roche Diagnostics; Mannheim, Germany). Amplification specificity was checked using a melting curve according to the manufacturer's instructions. The mRNA expression of each target was normalized to that of GAPDH. The forward and reverse primers are listed in Table 1.

Cell cultures

Cardiac fibroblasts were obtained from the ventricles of Wistar–Kyoto rats and grown in Iscove's modified

Table 1 Oligonucleotide primers used for real-time RT-PCR

Gene	Primers
Collagen type I	
Forward	5′-GCT TGG ATG GCT GCA C-3′
Reverse	5′-GGT GGG AGG GAA CCA GAT T-3′
Collagen type III	
Forward	5′-GGA AAA GAT GGA TCA AGT GGA C-3′
Reverse	5′-CTG GCT GTC CAG GGT GAC-3′
MCP-1	
Forward	5′-ATG CAG GTC TCT GTC ACG-3′
Reverse	5′-CAT TGG GAT CAT CTT GCC-3′
TN-C	
Forward	5′-ACC AAC TGT GCC CTG TCC TA-3′
Reverse	5′-GAT TTC GGA AGT TGC TGG GT-3′
ET-1	
Forward	5′-AGC TGG GAA AGA AGT GTA TC-3′
Reverse	5′-TCT GTA GAG TTC CGC TTT CA-3′
GAPDH	
Forward	5′-TAC ACT GAG GAC CAG GTT G-3′
Reverse	5′-CCC TGT TGC TGT AGC CAT A-3′

Dulbecco's medium (IMDM) supplemented with 10 % fetal bovine serum as described previously [34]. The experiments were performed on secondary cultures. Cells were plated in Multiwell 6-well plates (Becton–Dickinson, Franklin Lakes, NJ, USA) at 3×10^5 cells/well for 48 h in serum-free IMDM, and then treated with ET-1 (3×10^{-9}, 1×10^{-8}, 3×10^{-8}, and 1×10^{-7} mol/l) or Ang II (1×10^{-9} mol/l) for 6 h. To determine whether ET-1 is involved in the upregulation of Ang II-induced (1×10^{-9} mol/l) TN-C mRNA expression, the endothelin receptor (ET-R) antagonist bosentan (1×10^{-6} or 1×10^{-5} mol/l) was also used. To clarify the signaling pathways induced by Ang II, we coapplied the selective endothelin A receptor (ET-RA) antagonist BQ 123 (1×10^{-7}, 3×10^{-7}, and 1×10^{-6} mol/l) and/or the selective endothelin B receptor (ET-RB) antagonist BQ 788 (1×10^{-7}, 3×10^{-7}, and 1×10^{-6} mol/l). To examine if ANP blocks Ang II-induced TN-C expression, the cells were pretreated with ANP (1×10^{-8} or 1×10^{-7} mol/l) for 6 h and then stimulated with Ang II (1×10^{-9} mol/l) for 6 h. Total RNA was isolated from the treated cells using ISOGEN (Nippon Gene, Toyama, Japan), and the relative ET-1 or TN-C mRNA levels were determined by quantitative real-time RT-PCR.

Statistical analyses

All quantitative data are expressed as means ± standard deviation (SD). Numeric data were statistically evaluated by 1-way analysis of variance, followed by the Tukey–Kramer method for multiple comparisons. A P value less than 0.05 was considered to be statistically significant.

Results

Systolic blood pressure, heart rate, body weight, and heart weight/body weight ratio

The rats were subjected to Ang II infusion for 14 days, with or without administration of ANP. Compared with the controls (114 ± 5 mmHg), the Ang II and Ang II + ANP rats showed elevated SBP (Ang II, 204 ± 36 mmHg; Ang II + ANP, 201 ± 22 mmHg; $P < 0.001$). The Ang II rats had a significantly higher heart rate than the controls (control, 338 ± 12 beats/min; Ang II, 432 ± 53 beats/min; $P < 0.001$). In addition, the Ang II and Ang II + ANP rats had significantly lower body weights than the controls (control, 317 ± 18 g; Ang II, 216 ± 46 g; Ang II + ANP, 225 ± 45 g; $P < 0.001$). The Ang II rats had a significantly greater average heart weight/body weight ratio than the controls (control, 3.20 ± 0.55 mg/g; Ang II, 4.20 ± 1.02 mg/g; $P < 0.05$). The Ang II + ANP rats had a slightly, but not significantly, lower heart weight/body weight ratio compared with the Ang II rats (Ang II + ANP, 4.04 ± 0.78 mg/g; $P = 0.90$; Table 2). There were no significant differences between controls and ANP-alone rats in systolic blood pressure, heart rate, body weight, and heart weight/body weight ratio.

Ang II and Ang II + ANP rats showed comparable blood pressure and heart rate throughout the time course (Fig. 1).

Cardiac function

LVFS and EF were significantly lower in the Ang II rats than in the controls ($P < 0.001$), whereas the Ang II + ANP rats exhibited significantly higher LVFS and EF than the Ang II rats ($P < 0.001$). On the basis of Doppler spectra for

Table 2 Systolic blood pressure, heart rate, body weight, heart weight/body weight ratio, and echocardiographic parameters on day 14

	Control (n = 10)	Ang II (n = 10)	Ang II + ANP (n = 10)	ANP (n = 5)
Systolic blood pressure (mmHg)	114 ± 5	204 ± 36**	201 ± 22**	127 ± 5
Heart rate (beats/min)	338 ± 12	432 ± 53**	431 ± 76	352 ± 27
Body weight (g)	317 ± 18	216 ± 46**	225 ± 45**	306 ± 4
Heart weight/body weight (mg/g)	3.20 ± 0.55	4.20 ± 1.02*	4.04 ± 0.78	2.44 ± 0.11
LVDd (mm)	6.00 ± 0.35	4.14 ± 0.09**	4.36 ± 0.66	5.26 ± 1.20
LVDs (mm)	2.57 ± 0.37	2.12 ± 0.38*	1.83 ± 0.30	2.68 ± 0.77
EF (%)	92.1 ± 2.5	86.6 ± 2.5**	91.9 ± 2.1†	84.8 ± 8.8
FS (%)	57.9 ± 4.0	48.6 ± 3.1**	56.9 ± 4.1†	48.5 ± 10.3
E (cm/s)	0.78 ± 0.07	0.52 ± 0.08**	0.58 ± 0.09	0.61 ± 0.12
E/A	2.60 ± 0.27	1.98 ± 0.16**	2.13 ± 0.23	2.47 ± 0.41
DcT (ms)	67.4 ± 4.1	81.6 ± 5.5**	70.6 ± 3.0†	65.8 ± 4.8

Values are mean ± SD

LVDd left ventricular end-diastolic diameter, *LVDs* left ventricular end-systolic diameter, *EF* ejection fraction, *FS* fractional shortening, *E* peak velocity of mitral early inflow, *E/A* ratio of mitral early inflow peak velocity to atrial contraction-related flow peak velocity, *DcT* deceleration time

* $P < 0.05$ versus control, ** $P < 0.001$ versus control, † $P < 0.001$ versus Ang II

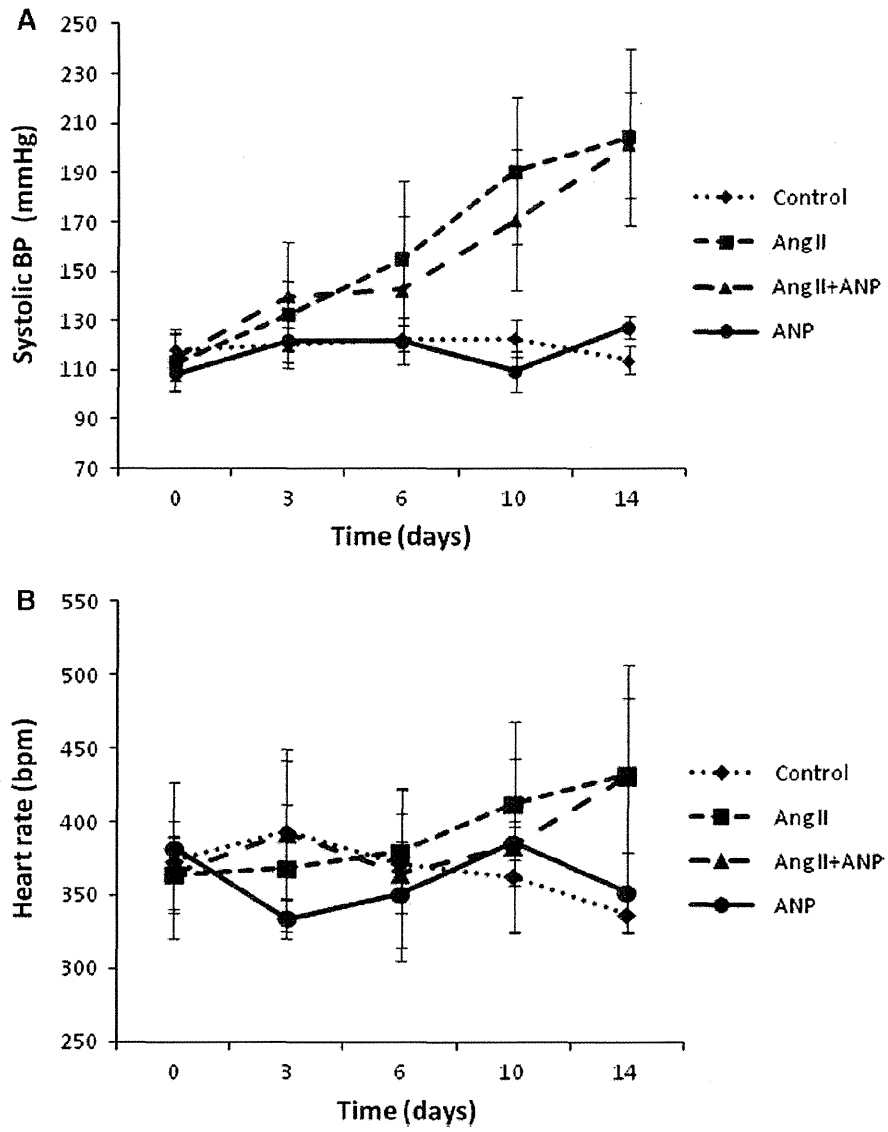

Fig. 1 The time course of systolic blood pressure (BP) (**a**) and heart rate (**b**). Values are expressed as mean ± SD. *Control* control rats, *Ang II* angiotensin II-treated rats, *Ang II + ANP* Ang II plus atrial natriuretic peptide-treated rats, *ANP* atrial natriuretic peptide-treated rats, *BPM* beats/min

transmitral flow, the Ang II rats showed significant decreases in *E* and *E/A* ratio, in addition to a significant prolongation of the DcT, compared with the controls (*E*, $P < 0.001$; *E/A*, $P < 0.001$; DcT, $P < 0.001$). Coadministration of ANP reversed the Ang II-mediated suppression of *E* and the *E/A* ratio, as well as the decreased DcT (*E*, $P = 0.22$; *E/A*, $P = 0.30$; DcT, $P < 0.001$; Table 2), indicating that ANP can partially reverse Ang II-induced ventricular dysfunction. There were no significant differences between controls and ANP-alone rats in echocardiographic parameters.

Myocyte hypertrophy

The average myocyte diameter was significantly greater in the Ang II rats than in the controls ($P < 0.001$). ANP coadministration significantly decreased myocyte diameter ($P < 0.01$; Fig. 2a, b). Compared with controls, the average myocyte diameter in ANP-alone rats showed no significant difference.

Myocardial fibrosis

The percent areas of myocardial fibrosis were significantly greater in the Ang II-treated rats than in the controls ($P < 0.001$). ANP coadministration significantly decreased interstitial fibrosis ($P < 0.01$; Fig. 3a, b). The mRNA levels of fibrotic indicators collagen type I (Fig. 3c) and collagen type III (Fig. 3d) were higher in the Ang II rats than in the controls, whereas ANP coadministration significantly decreased the mRNA levels of collagen type I (Fig. 3c) and collagen type III (Fig. 3d).

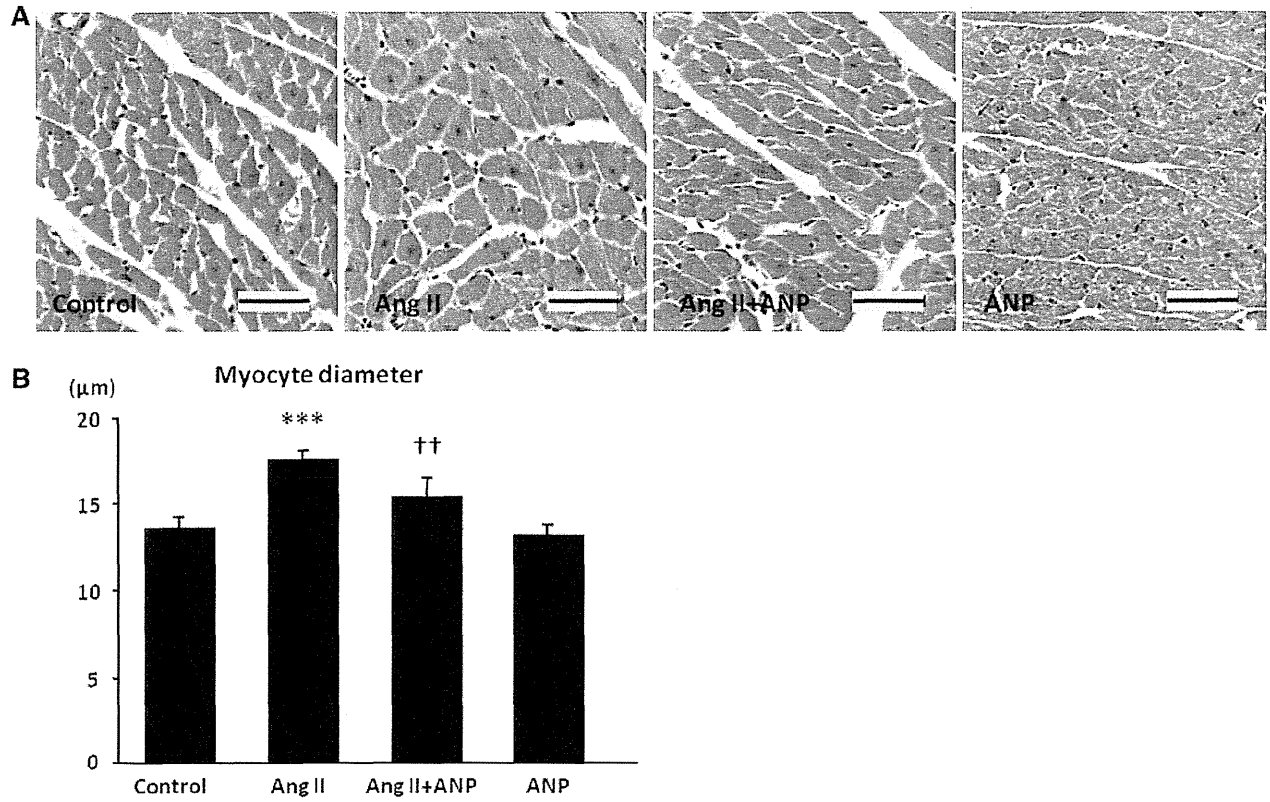

Fig. 2 Histological changes in the rat myocardium induced by chronic Ang II infusion. **a** Light micrographs of hematoxylin–eosin-stained sections (*scale bar* 50 μm). **b** The diameter of the myocytes. Values are expressed as mean ± SD. *Control* control rats, *Ang II* angiotensin II-treated rats, *Ang II + ANP* Ang II plus atrial natriuretic peptide-treated rats, *ANP* atrial natriuretic peptide-treated rats. $^{***}P < 0.001$ vs. the control group, $^{\dagger\dagger}P < 0.01$ vs. the Ang II group

Compared with controls, the percent areas of myocardial fibrosis in ANP-alone rats showed no significant difference. In addition, the mRNA levels of collagen type I and collagen type III of ANP-alone rats also showed no significant difference.

Cardiac inflammation

Immunostaining for TN-C is shown in Fig. 4a. The average TN-C-positive area was larger in the Ang II rats than in the controls, and again TN-C immunoreactivity was decreased by ANP coadministration. Similarly, the total number of CD68-positive cells per unit area (1 mm^2) was significantly greater in the Ang II rats than in the controls ($P < 0.001$; Fig. 4b, d). This increase was significantly decreased by ANP coadministration ($P < 0.05$; Fig. 4b, d). mRNA levels of TN-C (Fig. 4c) and MCP-1 (Fig. 4e) were increased in the Ang II rats compared with the controls, whereas ANP coadministration significantly decreased both TN-C (Fig. 4c) and MCP-1 (Fig. 4e) mRNA levels. Compared with controls, TN-C-positive area and the total number of CD68-positive cells in ANP-alone rats showed no significant difference. In addition, the mRNA levels of TN-C and MCP-1 of ANP-alone rats also showed no significant difference. The mRNA level of ET-1 was higher in the Ang II rats than in the controls. The mRNA level of ET-1 was decreased in the Ang II + ANP rats compared with the Ang II rats, but the difference was not statistically significant ($P = 0.38$, data not shown).

Confocal laser scanning microscopy

In the fibrotic area shown in Fig. 4a, b, by confocal laser scanning microscopy a large number of CD68-positive macrophages and α-SMA-positive cells, presumably myofibroblasts, was observed. We then compared whether TN-C immunopositivity colocalized with CD68 and α-SMA positivity. Most of the α-SMA-positive cells were found to be negative for TN-C staining (Fig. 5a), and CD68-positive macrophages were negative for TN-C staining (Fig. 5b).

Effects of ANP on TN-C synthesis by cardiac fibroblasts in culture

The effects of Ang II on TN-C and ET-1 gene expression, and the role of ET-1 receptors in Ang II- and ANP-mediated regulation of TN-C gene expression, were

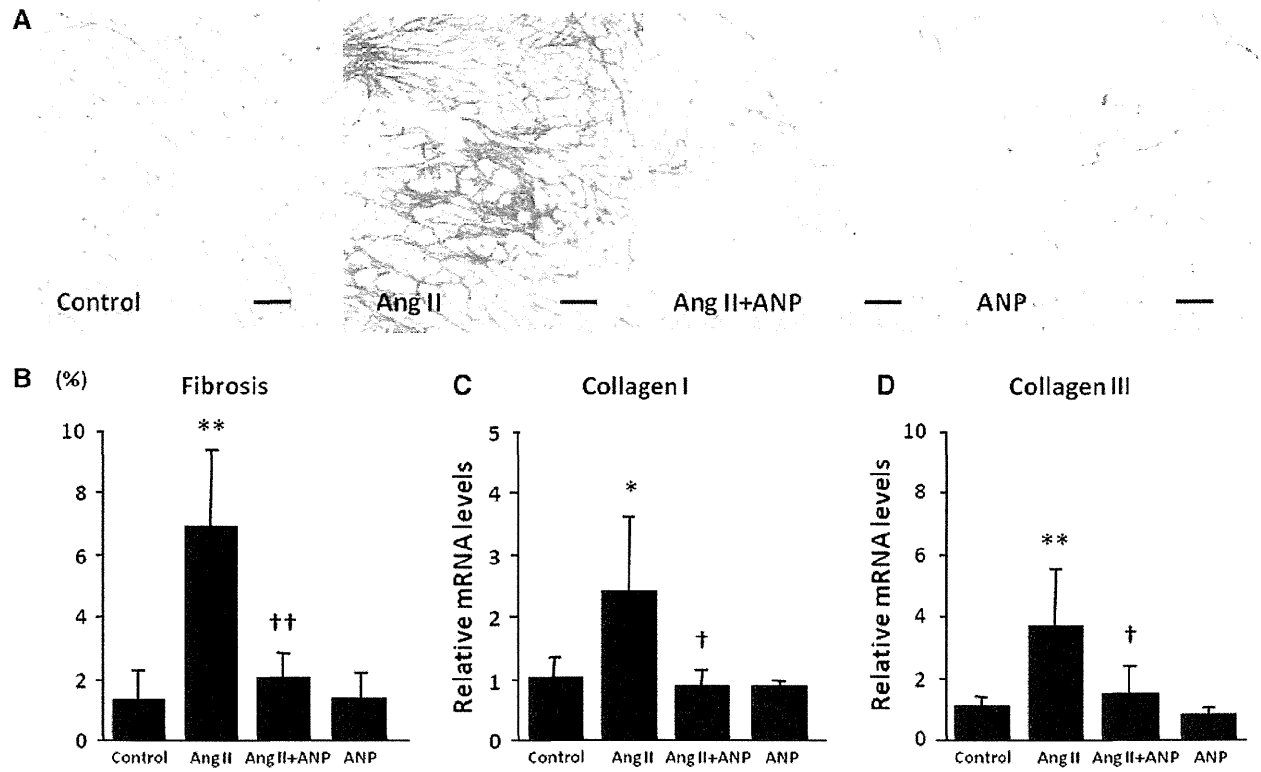

Fig. 3 Histological features of Ang II-induced myocardial fibrosis. **a** Light micrographs of Sirius Red staining (*scale bar* 100 μm). **b** Percent area of myocardial interstitial and perivascular fibrosis. **c** Relative mRNA levels of collagen I. **d** Relative mRNA levels of collagen III. Values are expressed as mean ± SD. *Control* control rats, *Ang II* angiotensin II-treated rats, *Ang II + ANP* Ang II plus atrial natriuretic peptide-treated rats, *ANP* atrial natriuretic peptide-treated rats. $^{*}P < 0.05$, $^{**}P < 0.01$ vs. the control group, $^{\dagger}P < 0.05$, $^{\dagger\dagger}P < 0.01$ vs. the Ang II group

examined in cultured cardiac fibroblasts by quantitative real-time RT-PCR. Ang II administration increased TN-C mRNA expression, and ANP coadministration significantly reversed this upregulation (Fig. 6a). In addition, Ang II increased ET-1 mRNA expression, whereas ANP coadministration significantly reversed this upregulation (Fig. 6b). Treatment of cultured cells with ET-1 significantly increased TN-C mRNA expression in a dose-dependent manner (Fig. 6c). Upregulation of Ang II-induced TN-C mRNA expression was significantly blocked by the ET-R antagonist bosentan and the ET-RA antagonist BQ123 (Fig. 6d, e), but not by the ET-RB antagonist BQ 788 (Fig. 6f).

Discussion

The present study clearly demonstrated that ANP treatment attenuates Ang II-induced cardiac inflammation, fibrosis, and hypertrophy, and improves systolic and/or diastolic cardiac function of the rat model.

It has been suggested that ANP may inhibit adverse cardiac remodeling by preventing cardiomyocyte hypertrophy and fibrosis based on G kinase activation [19, 35–37] in experiments using cultured cells and a natriuretic peptide receptor-deficient mice [38–40]. In our present study, ANP administration to rats significantly reversed Ang II-induced myocyte hypertrophy and fibrosis, which supports previous findings. Furthermore, we found that ANP obviously reduced infiltration of macrophages as well as expression of TN-C, an inflammatory marker, induced by Ang II administration.

The clinical significance of RAAS-mediated chronic myocardial inflammation is well recognized (reviewed in [41]). Inflammation and fibrosis are closely related; indeed, multiple factors associated with chronic inflammation are believed to induce fibrosis. Among these factors, matricellular proteins, a category of extracellular matrix molecules, have attracted considerable attention [31, 42]. Matricellular proteins do not contribute to the formation of fibers or basement membrane but rather serve as biological mediators by interacting directly with cells or regulating the activities of growth factors, cytokines, proteases, and other extracellular matrix proteins [43, 44]. TN-C is a typical matricellular protein expressed transiently at restricted sites during embryonic development, tissue

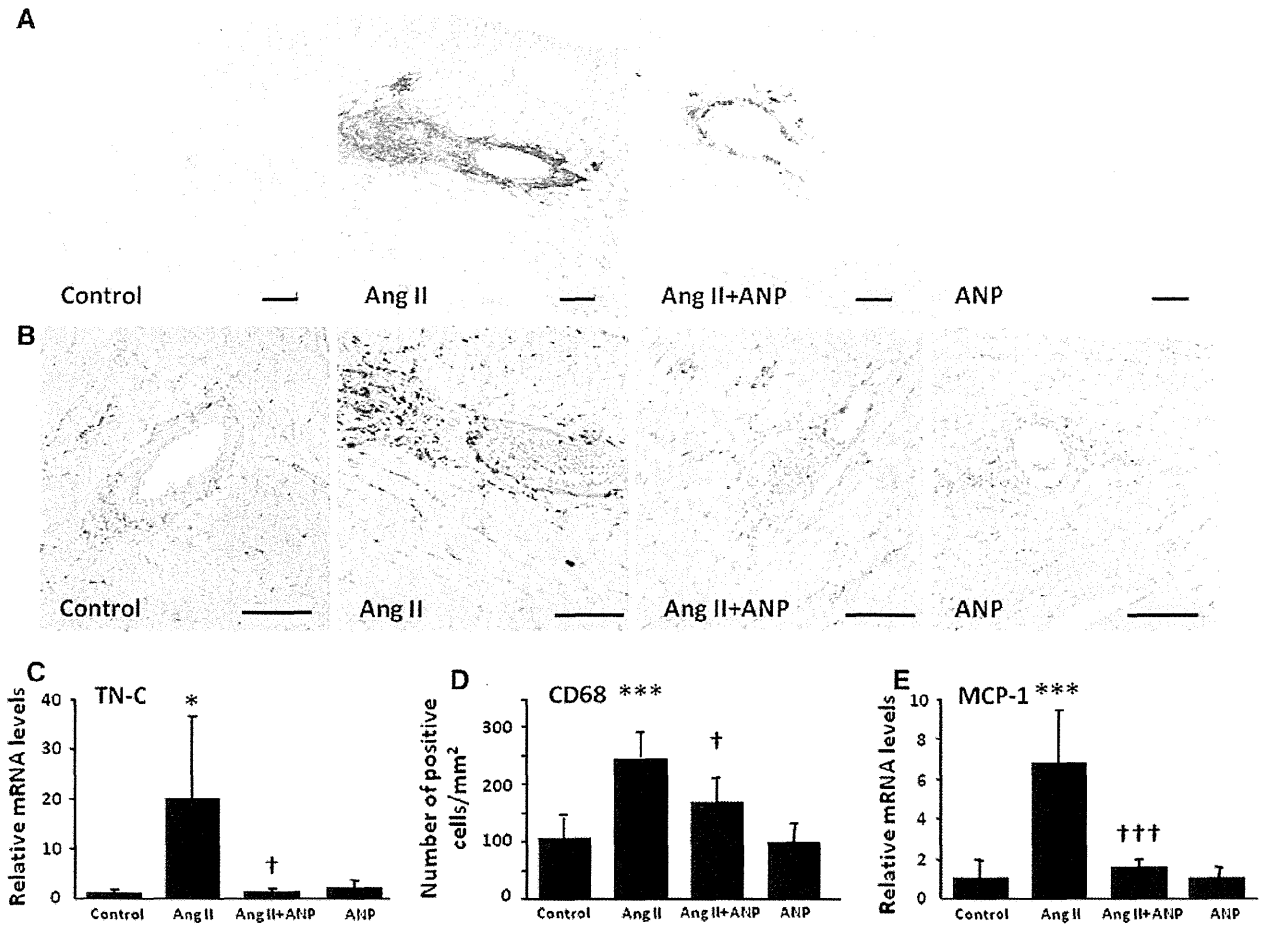

Fig. 4 **a** Changes in TN-C immunoreactivity in response to Ang II (*scale bar* 100 μm). **b** Immunostaining for CD68 (*scale bar* 100 μm). **c** Relative mRNA level of TN-C. **d** Total number of CD68-positive cells per unit area (1 mm^2). **e** Relative mRNA level of MCP-1. Values are expressed as mean ± SD. *Control* control rats, *Ang II* angiotensin II-treated rats, *Ang II + ANP* Ang II plus atrial natriuretic peptide-treated rats, *ANP* atrial natriuretic peptide-treated rats. $^{*}P < 0.05$, $^{***}P < 0.001$ vs. the control group, $^{\dagger}P < 0.05$, $^{\dagger\dagger\dagger}P < 0.001$ vs. the Ang II group

injury, inflammation, and fibrosis [45, 46]. Several lines of evidence suggest that TN-C could act as a profibrotic and proinflammatory modulator by enhancing macrophage activity [31, 47, 48]. In fact, deletion of the TN-C gene in mice attenuates hepatitis and liver fibrosis [49], rheumatoid arthritis [50], and fibrosis after myocardial infarction [51].

Several reports have suggested that ANP may have an anti-inflammatory effect [52, 53] and may inhibit macrophage activity [54]. We proposed that ANP may weaken inflammation by downregulation of TN-C, a modulator of inflammation.

In general, major sources of TN-C in myocardium could be the interstitial fibroblasts, as we have previously reported [25, 33]. Ang II upregulates TN-C expression in cultured cardiac fibroblasts as well as proinflammatory cytokines, growth factors, and reactive oxygen species [28]. We speculate that Ang II may stimulate interstitial fibroblasts to induce TN-C expression, which is reduced by ANP.

Using cultured cardiac fibroblasts, we found that ANP suppressed TN-C expression induced by Ang II. We investigated the role of ET-1 in Ang II/TN-C signaling because several recent studies have linked ET-1 to fibrosis, inflammation, and cardiovascular remodeling in the downstream signaling of Ang II [55]. Furthermore, it is well known that ANP suppresses gene expression of ET-1 of cardiac fibroblasts, as an autocrine/paracrine factor [56, 57], attributable to G kinase [56]. We first confirmed that Ang II upregulated ET-1 expression, which was suppressed by ANP, as reported previously [56]. Second, we examined if ET-1 is involved in TN-C upregulation by Ang II in fibroblasts. Dual ET-R and ET-RA blockade significantly suppressed TN-C upregulation, whereas ET-RB blockade did not. Conversely, ET-1 increased TN-C expression. Taken together, these in vitro results suggested that ANP may suppress Ang II-induced TN-C synthesis, at least in part, by inhibiting the ET-1/ET-RA signaling